ADDIS ABABA UNIVERSITY

SCHOOL OF GRADUATE STUDIES

DEPARTMENT OF CHEMISTRY

EFFECT OF LOW BOILING POINT SOLVENT ADDITIVES ON THE PHOTOVOLTAIC PERFORMANCE OF TQ1:$PC_{61}BM$ BASED BULK HETEROJUNCTION SOLAR CELLS

BY: HAGOS TUKUE

ADVISOR: PROF. TEKETEL YOHANNES

JUNE, 2014

Effect of Low Boiling Point Solvent Additives on the Photovoltaic Performance of TQ1:$PC_{61}BM$ Based Bulk Heterojunction Solar Cells

A Thesis

Submitted to the Department of Chemistry

School of Graduate Studies

Addis Ababa University

Presented in the Partial Fulfillment of the Requirements for the Degree of

Master of Science

In

Physical Chemistry

By

Hagos Tukue

Advisor: Prof. Teketel Yohannes

DECLARATION

I, the undersigned, declare that this thesis submitted to the Addis Ababa University for the degree of Master of Science in Chemistry in the School of Graduate Studies, and this thesis represents my own work under the supervision of Prof. Teketel Yohannes. This thesis has not been previously included in a thesis, dissertation or report submitted to this University or to any other institution for a degree, diploma or other qualifications.

Name: Hagos Tukue

Signature: _____

Date:_____

Effect of Low Boiling Point Solvent Additives on the Photovoltaic Performance of TQ1:$PC_{61}BM$ Based Bulk Heterojunction Solar Cells

By: Hagos Tukue

Addis Ababa University

Department of Chemistry

Approved by the Examining Board

	Signature	Date
Prof. Teketel Yohannes (Advisor)	_____	_____
Prof. Theodros Solomon (Examiner)	_____	_____
Dr. Mesfin Redi (Examiner, Chairperson)	_____	_____

_____

Chair of Department or Graduate Program Coordinator

ABSTRACT

The need for clean, inexpensive and renewable energy has increasingly turned research attention towards polymer photovoltaic cells. However, the performance efficiency of these devices is still low in comparison with silicon-based devics. The recent introduction of solvent additives has resulted in a remarkable increase in power-conversion efficiency by controlling the interpenetrating network morphology of the organic bulk heterojunction solar cells. In this study the effect of low boiling point solvent additives such as iodomethane, iodoethane and di-iodomethane on the photovoltaic porformance of TQ1:$PC_{61}BM$ (1:2) based organic BHJ solar cells with the device architecture glass/ITO/PEDOT-PSS/TQ1:$PC_{61}BM$/Al were studied. It was shown that the highest PCE of 4.53% was obtained by solar cell made from a blend solution containing 3% (v/v) di-iodomethane. Similarlly, devices made from blend solutions containing 3% (v/v) of iodomethane and iodoethane exhibited PCE of 3.28 and 3.76%, respectively. The addition of these solvent additives has mainly increased the short-circuit current density (J_{sc}) of the solar cells compared to pristine TQ1:$PC_{61}BM$ based solar cell. As confirmed from UV-Vis absorption and photoluminescence spectra, addition of these solvent additives has enhanced photon absorption and photoluminescence quenching efficiency, respectively. Hence, this study have shown that despite the high boiling point solvent additives, low boiling point solvent additives can improve the phase separation of the active layer that in turn enhances charge dissociation and PCE.

Key words:

Energy Conversion, Organic Solar Cells, Bulk Heterojunction, TQ1, Solvent Additives

ACKNOWLEDGEMENTS

First and foremost, I would like to express my deepest gratitude to my supervisor Prof. Teketel Yohannes, who have given me the great opportunity to study on organic photovoltaics solar cell and let me join his group. Thanks for your excellent guidance, caring, patience and providing me with an excellent atmosphere for doing my research.

Next, I owe a special thanks to Bedasa Abdisa, for his unforgettable assistance, day to day follow up, guidance, valuable suggestions, encouragement, inspiring and helpful discussions during the entire period of this study. Furthermore, I want to thank Fedlu Kedir and Endale Tsegaye for their unlimited assistance and moral support. My thanks also goes to Dawit Tibebu, my labmate, for helping every work in the experiment.

My exceptional thank also goes to Prof. Wendmagegn Mamo for allowing me to use Spin coater. I am greatful to Dr. Ahmed Mustefa for his day to day advice and encouragement through out the year.

My special thanks extends to Department of Chemistry, Addis Ababa University for sponsoring my study and I strongly acknowledge DAAD in Country Scholarship Provider for supporting a financial aid during my study.

Finally, I would like to acknowledge my mother, brother (G/Hiwot Tukue) and his sons (Abel, Hebros and Nahom), and my friends for providing me supports with out reservation.

Hagos Tukue

Addis Ababa, Ethiopia.

TABLE OF CONTENTS

LIST OF FIGURES

LIST OF TABLES

LIST OF ABBREVIATIONS

AM	Air mass
BHJ	Bulk heterojunction
DIMe	Di-iodomethane
EQE	External quantum efficiency
E_g	Energy bandgap
FF	Fill factor
HOMO	Highest occupied molecular orbital
IEt	Iodoethane
IMe	Iodomethane
IPCE	Incident photon-to-current conversion efficiency
ITO	Indium doped tin oxide
J_{max}	Maximum current density
J_{sc}	Short-circuit current density
J-V	Current density-Voltage
LUMO	Lowest unoccupied molecular orbital
MPP	Maximum power point
OPV	Organic photovoltaics
o-DCB	ortho-Dichlorobenzene
$PC_{61}BM$	Phenyl-C_{61}-butyric acid methyl ester
PCE, (η)	Power conversion efficiency
PEDOT-PSS	Poly (3,4-ethylenedioxythiophene)-Poly(4-styrensulfonate)
PL	Photoluminescence

P_{max}	Maximum power
PSC	Photovoltaic solar cell
RPM	Revolution per minute
TQ1	Poly[2,3-bis-(3-octyloxyphenyl)quinoxaline-5,8-diyl-alt thiophene-2,5-diyl]
UV-Vis	Ultraviolet Visible
V_{oc}	Open-circuit voltage
V_{max}	Maximum Voltage

1. INTRODUCTION

Energy and health care are two important areas for human beings and directly related to well-being. The energy demand of our world is increasing rapidly due to increasing human population, urbanization, and modernization. Currently, close to 80% of the energy supply worldwide is based on fossil fuels like coal, oil and gas which are not renewable sources [1]. Nowadays, one of humanity's major challenges is the development of renewable energy sources to secure our current lifestyle [2]. Due to the depletion of fossil fuels and the dramatic increase in price of oil and gas, renewable energy sources such as solar and wind energies have drown great attention both by industry and academic institutions.

Among the renewable sources of energy, the Sun provides a reliable, sustainable, clean, and long-term supply of energy, in contrast to conventional resources such as coal and fossil fuels, and can therefore help to solve the growing global need for energy [3, 4, 5]. To date, more energy from sunlight strikes the Earth in one hour (4.3×10^{20} J) than all the energy consumed on the planet in a year (4.1×10^{20} J). This indicates that there is a huge gap between our present use of solar energy and its potential, which defines the grand challenge in energy research [6]. The ever increasing demand for clean energy has prompted researchers to intensively investigate environmentally friendly photovoltaic devices [7]. One effective method of converting solar energy into a useful form like electricity is the photovoltaic effect [8].

Solar cells are photovoltaic devices, which convert electromagnetic radiation from the sun to electricity without “green house” gas emission. Solar cells of different technologies have gained a lot of interest during the last decades. The most commonly used solar cell technology is silicon based solar cells. Daryl Chapin et al. [9] fabricated the first practical solar cell based on a Si (silicon) p-n junction in 1954 at Bell Laboratories. This solar cell exhibited a power conversion efficiency of ~6% . Since then, solar cell technology has been rapidly developing in both academia and industry. Today, the power conversion efficiencies of the best single junction and multi-junction silicon-based solar cells reach 28.8% and 37.9%, respectively [10]. For commercial mono-crystalline inorganic solar cells, the power conversion efficiency is ~22% [11].

However, the wide spread expansion in the use of conventional solar cells based on semiconductor substrate such as Si, GaAs, etc. remains limited because of the high costs imposed by fabrication procedures involving elevated temperatures, high vacuum, and numerous steps [4]. The development of new solar cell technologies with lower production costs (through the use of abundant materials and inexpensive processes) is therefore of great interest to industry [5]. Fore that reason, considerable research efforts have been put into the development of alternative solar cell technologies and large improvements have been achieved in the last 10 - 20 years [12].

One of the alternatives to high cost inorganic based solar cells are organic solar cells. Organic solar cells, based on conjugated polymers, can be easily processed at room temperature using inexpensive technologies, which makes them an attractive alternative to the expensive inorganic solar cells [13]. Moreover, as the absorption coefficient of organic film is high the films can be made into thin panels and have added advantage of

being flexible (are mechanically flexible devices). Although there has been fast development of the organic solar cell field with device efficiency improving from less than 1% [14] to over 12% [15] within the last few years, the efficiency is still very low compared to inorganic photovoltaics. Therefore, the main limitations associated with organic photovoltaic cells compared to inorganic solar cells are low efficiency, low stability and low strength [16]. However, combined with the flexibility of organic molecules films, OPV cells are potentially cost-effective and promising for photovoltaic applications.

Aim and outline of the thesis

In this thesis the factors affecting the nanomorphology of bulk heterojunction solar cells particularly solvent additives will be examined to see the effect on photovotaic parametrs.

2. LITERATURE REVIEW

2.1 Conducting Polymers

Polymers are macromolecules consisting of a great number of repeating units, which are coupled to each other by covalent bonds to form a long chain. These repeating units can be any group of atoms; however, we consider only organic polymers, where the backbone consists of only carbon atom. Conventional polymers, plastics, have been used traditionally because of their attractive chemical, mechanical, and electrically insulating properties, and not for their electronic properties.

One class of the organic compounds, which effectively transport charges, are electronically conducting polymers [17]. Electronically conducting polymers contain π-electron backbone (alternating single and double bonds), which is responsible for their unusual electrochemical properties (high electrical conductivities, low ionization potentials and high electron affinities), and optical properties (low energy optical transitions), previously observed in inorganic materials [18]. Figure 2.1 shows the chain of the carbon atoms with the alternating single and double bonds which are responsible for origin of the conductivity and semi-conductivity behavior.

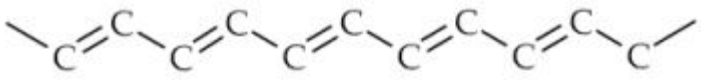

Figure 2.1: The chain of the carbon atoms with the alternating single and double bonds.

The higher values of the electrical conductivity obtained in such organic polymers have led to the name ‘synthetic metals’ or ‘semiconductors’. Nowadays conjugated polymers are used in various applications, like transistors, photodiodes, light emitting diodes, solar cells, etc [19].

The carbon atom, in the ground state, has four valence electrons, 2 in 2s and 2 in 2p orbitals. In conjugated polymers, carbon atoms are sp^2 hybridized. In the sp^2 hybridization the 2s orbital is hybridized with two 2p orbitals ($2p_x$, $2p_y$) giving rise to three sp^2 orbitals and one 2p orbital ($2p_z$) is left unhybridized. Carbon can form two types of bonds: namely σ and π bonds. The σ bond is formed by the overlap of the hybridized orbitals of the adjacent atoms which are oriented along the chain. So, there are three coplanar sp^2 hybridized orbitals which are at an angle of 120° with each other. Therefore, three σ bonds are formed; two with neighboring carbon atoms and one with a hydrogen atom (in ethylene). The remaining out of plane p_z orbitals, each occupied by one electron, overlap with neighboring p_z orbitals to form π-bonds which are perpendicular to the chain as shown in Figure 2.2. These electrons are delocalized along the entire polymer backbone, which is the reason for the conducting properties of conjugated polymers [20]. The overlap of p_z orbitals forms two molecular orbitals, a bonding π orbital which is the highest occupied molecular orbital (HOMO) and an antibonding π^* orbital which is the lowest unoccupied orbital (LUMO). The π orbital and π^* orbital are equivalent to the valence band and conduction band of an inorganic semiconductor, respectively. The difference between the HOMO and LUMO is called the bandgap of the organic material. This bandgap determines the optical and electrical properties of an organic material. The bandgap is reduced when the polymer chain is getting longer.

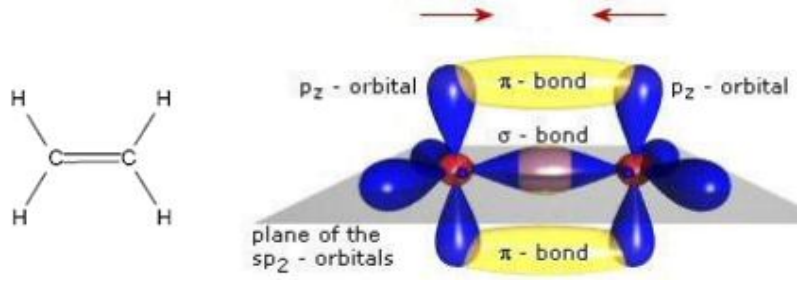

(a) (b)

Figure 2.2: The chemical structure (a) and schematic drawing (b) of ethylene.

Figure 2.3 shows the energy levels of a π-conjugated molecule and collection of molecular orbitals (bands) separated by an energy gap.

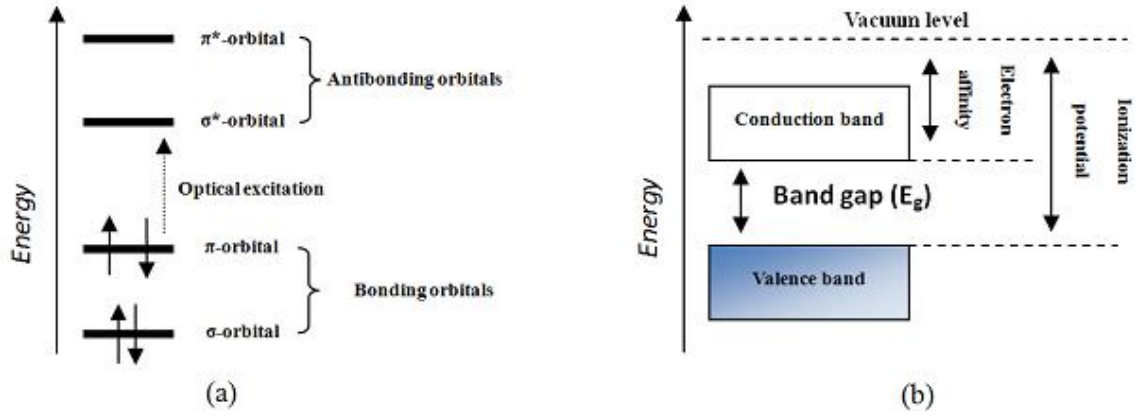

Figure 2.3: (a) The energy levels of a π-conjugated molecule, the lowest electronic excitation is between the bonding π-orbital and the antibonding π*-orbital, (b) collection of molecular orbitals form bands separated by an energy gap.

Figure 2.4 shows some of the common conducting polymers.

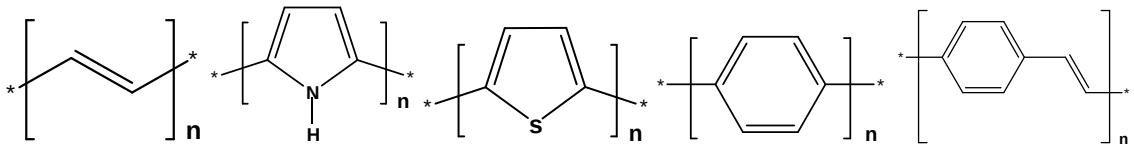

(I) (II) (III) (IV) (V)

Figure 2.4: The chemical structure of common polymers chains: polyethylene (I), Polypyrrole (II), Polythiophene (III), Polyphenylene (IV) and Poly(para-phenylene vinylene) (V).

The main chain of conducting polymers is decorated with side chains to promote solubility in common solvents and to facilitate chain packing in solid films. Addition of side chains also reduces melting temperature, enhances flexibility, and reduces intermolecular overlap of neighbouring chains [21].

2.2. Conduction Mechanism in Conjugated Polymers

Materials according to conduction properties can be classified as conductors, semiconductors and insulators. Conducting materials, e.g. metals, do not possess a bandgap since there is no energetic difference between the valence and the conduction band. For an insulating material, this difference between these energy levels is large and it is therefore more difficult to excite the electrons from HOMO to LUMO.

Conjugated polymers can be oxidized or reduced more easily and reversibly than conventional polymers. The effect of this oxidation or reduction on polymer is called doping. Doping is one mechanism of enhancing electrical conductivity of conjugated polymers [22].

Generally, doping can be accomplished through chemical and electrochemical processes. For example, chemical doping increases conductivity of the organic or polymeric conductor, either by partially oxidizing the electron acceptors (p-doping) or by reduction of the electron donor (n-doping). Heeger, Mac Diarmid and Shirakawa demonstrated in 1977 that chemical doping of conjugated polymers results in an increase of electronic conductivity by several orders of magnitude. This discovery was awarded with the Nobel Prize in chemistry in 2000 [23]. Electrochemical doping corresponds to the removal or addition of electrons at the interface of an electrode. Dopant ions form during the electron transfer reaction or as the original component of the system.

The successful mechanism of doping in conductivity enhancement is explained in Figure 2.5. In organic conductors, there is a finite energy gap that separates the HOMO (valence band), and LUMO (conducting band). This energy gap (E_g), corresponds to the energy that must be applied to the system to induce charge mobility. The p-doping process removes one electron from the HOMO, and thus the HOMO level increases while E_g decreases. For the n-doping process, one electron is added to LUMO and lowering its energy level which results in decreasing E_g. In this manner, both p-doping and n-doping decrease E_g and hence increase the conductivity [24].

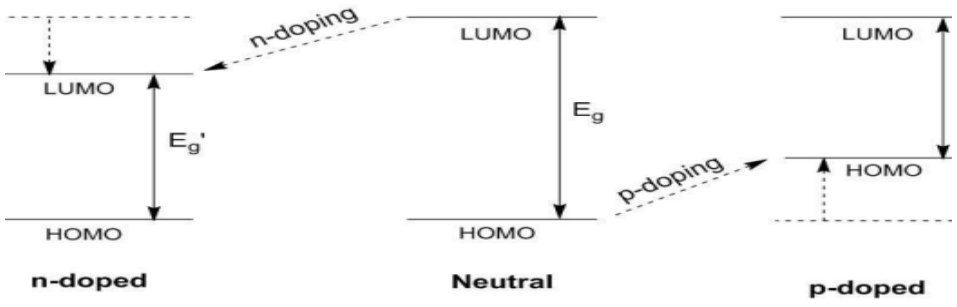

Figure 2.5: Molecular orbital energy diagram of organic conductor and effect of doping.

2.3 Device Structure of Organic Solar Cells

This third generation PV cell technology uses organic, electronic conductive polymers or small molecules for light absorption and electrical charge transport. The benefits are low cost and large scale production capability with flexibility. The disadvantages are low efficiency, low stability, and low strength compared to traditional non-organic PV cells [25]. Various active layer architectures have been explored since the introduction of polymer solar cells such as single layer, bilayer and bulk heterojunction solar cells. In the following, these three different forms of device architecture will be discussed.

2.3.1 Single Layer Organic PV Cells

Single layer is the simplest organic photovoltaic device structure, also known as a homojunction device (Figure 2.6). The first organic solar cells were based on an active layer made of a single material, sandwiched between two electrodes of different work functions. The front electrode is a thin transparent layer of metal or transparent conducting oxide such as Indium Tin Oxide (ITO) which have high work function while the back electrode is a metal with a relatively low work function (Al, Mg, Ca). Once an external circuit is made by connecting the two electrodes with a conductor, the difference in the work functions creates an electric field in the organic layer. Upon absorption of light, the electrons are excited to the LUMO leaving hole in the HOMO, forming excitons (strongly coulomb-bound electron–hole pairs) (Figure 2.6). The electric field in the organic layer will therefore help to break up the exciton pairs, pulling electrons to the positive electrode and holes to the negative electrode. Figure 2.6 shows schematic diagram of single layer organic solar cell, and process of photocurrent extraction. For

single layer device to generate electricity, light is obserbed by the single active material (polymer) first and followed by exciton formation. The exitons formed are then diffused to the interface of polymer and low work function electrode (Al), and get dissociated due to an electric field formed as a a result of the work function difference of the two electrodes. Finally, the generated free charges are collected by corresponding electrodes (hole by anode (ITO) and electrons by cathode (Al)).

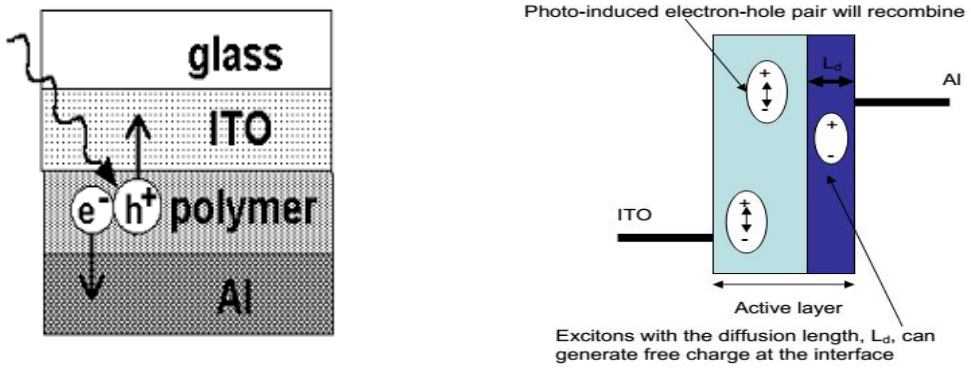

(a) (b)

Figure 2.6: (a) Schematic diagram of single layer organic solar cell, (b) Process of photocurrent extraction.

This class of solar cell though simple to fabricate has low quantum efficiency and conversion efficiency below 1% [26]. The drawback is because of the electric field (in the organic layer) resulting from the difference in work functions of the two electrodes is usually not sufficient to achieve an effective separation of the exciton pairs. Therefore, not all excitons are dissociated, but can as well recombine radiatively and emit energy as light by photoluminescence.

2.3.2 Double Layer (or Bilayer) Organic PV cells

The double layer organic solar cell improves the functionality of the single layer OPVs by including a distinct organic donor layer and a distinct acceptor layer between the two anode and cathode electrodes with a planar interface as shown in Figure 2.7. Bilayer solar cell uses higher electron affinity and ionization potential electron acceptor besides to the electron donor. These two layers of materials have differences in electron affinity and ionization energy. As a result, electrostatic forces are generated at the interface between the two layers and results in charge transfer and exciton dissociation in bilayer heterojunction. Finally, the holes travel to the anode though the donor material and the electrons travel to the cathode in the acceptor material. Charge recombination in double layer is less than in single layer photovoltaic cells. The reason is due to the local electric fields formed in the bilayer that may break up the excitons more efficiently [27]. Figure 2.7 shows schematic diagram of bilayer organic solar cell, and process of photocurrent extraction. First, light is obserbed by the electron donor active material (polymer) and exciton formation.Then, the exitons are diffused to the electron donor- acceptor interface. After the excitons are reached at the inteface charge transfer from donor to acceptor and dissociation of exitons at the D-A interface will be takes place. Then, the generaed free hole and electron are transported through the electron donor and acceptor, respectively to the corresponding electrodes, hole to anode and electron to cathode.

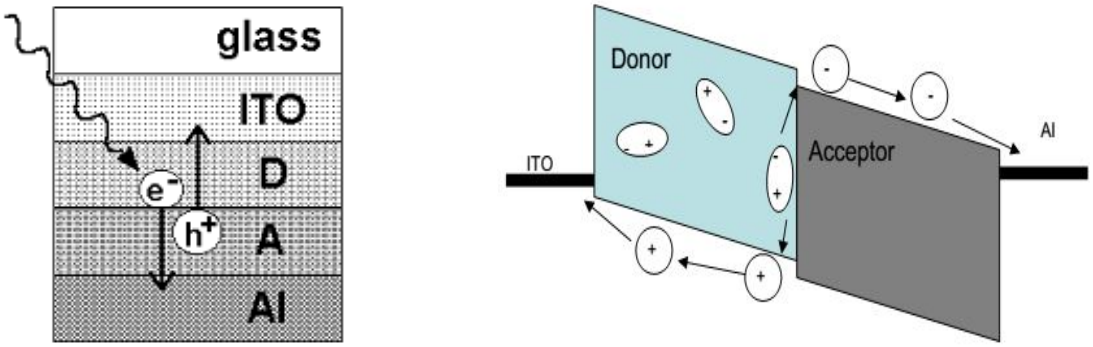

(a) (b)

Figure 2.7: (a) Schematic diagram of bilayer organic solar cell, (b) Process of photocurrent extraction.

The first organic bilayer solar cell was presented by Tang in the mid-1980s [28], made of two conjugated small molecules, and achieved a power conversion efficiency of about 1%. The main problem of these heterojunction devices is the short diffusion length of exciton in these materials due to small interface area. The diffusion length of excitons in polymers is about 10 - 20 nm. For effective dissociation of excitons, the thickness of the layers must be in the same range as this diffusion length. However, the organic material layer needs a minimum thickness of 100 nm to absorb enough photons [29].

2.3.3 Blend Layer (or Bulk Heterojunction) Organic PV Cells

The planar donor-acceptor junction increases the active region of the solar cell with respect to the single layer device, which is still usually not enough for efficient light absorption. To overcome this problem and to increase the optical thickness of the film while maintaining efficient current collection at the same time, the concept of interpenetrating network of electron accepting and electron-donating molecular species was developed and demonstrated [25]. Today, the most commonly used architecture is

the so-called bulk heterojunction (BHJ). The bulk heterojunction device is similar to the bilayer device with respect to the D-A concept. However, the two components (donor and acceptor materials) are intimately mixed in one layer (Figure 2.8) and phase separation of the donor/acceptor occurs in the bulk.

Solution-processed bulk-heterojunction (BHJ) solar cells were first reported by Friend et al. with all polymer active thin films [30] and followed by Heeger et al. in 1995 with a polymer/fullerene composite [31] and it has been shown to be superior to earlier architectures. Compared to the bilayer architecture, the interpenetrated network of BHJ: (a) minimizes the travelling distance of excitons (electron-hole pair generated upon light absorption, (b) provides larger interfacial area between the donor and the acceptor material, thereby ensuring the exciton dissociation to generate maximum free charge carriers, and (c) offers the formation of the charge-transfer state, and facilitate the charge collection at electrodes [32]. Figure 2.8 shows schematic diagram of hulk heterojunction organic solar cell, and process of photocurrent extraction. Similar to double layer devices, light is obserbed by the donor–acceptor active layer first and followed by exciton formation.Then, the exitons formed are diffused to the electron donor-acceptor interface for charge transfer from donor to acceptor due to the electric field produced by the LUMO-LUMO offsets of the donor and acceptor in the belnd. The generaed free hole and electron are then transported through the electron donor and acceptor to respective electrodes.

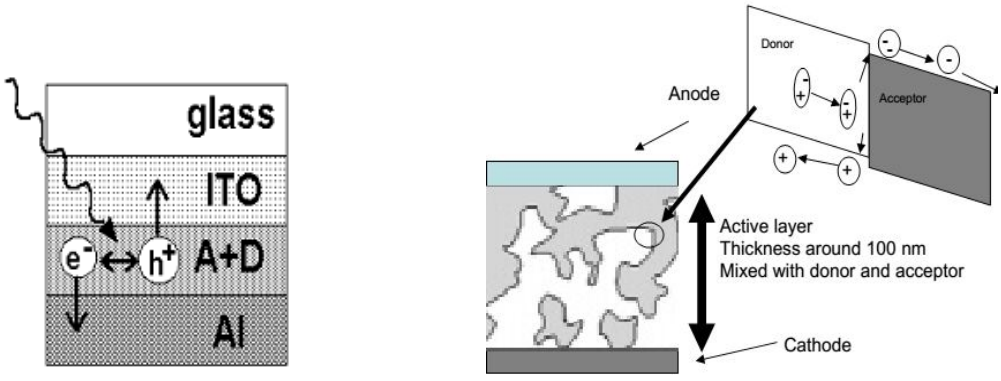

(a) (b)

Figure 2.8: (a) Schematic diagram of bulk heterojunction device, (b) Process of photocurrent extraction.

A continuous pathway is preferred for transportation of the free charge carriers to the electrode. Therefore, the bulk heterojunction devices are sensitive to the nanoscale morphology in the blend. Figure 2.9 shows the summary of schematic comparison of single layer, bilayer, and organic BHJ solar cells.

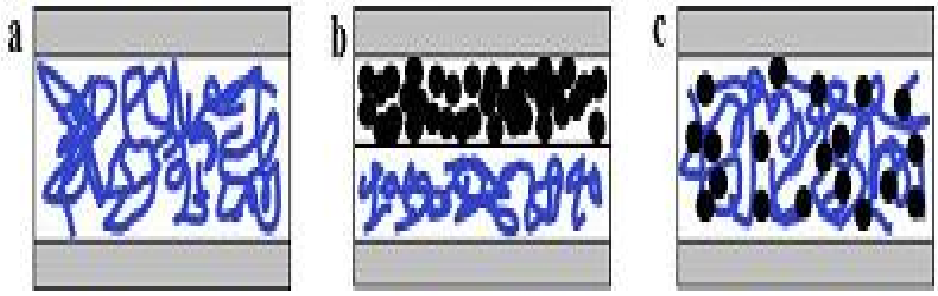

Figure 2.9: Schematic comparison of solar cell architectures; (a) single layer (b) bilayer and (c) BHJ with polymer- (blue) and PCBM-rich (black) phases.

2.4 Working Principle of Organic BHJ Polymer Solar Cells

Organic solar cells are built from thin films of organic semiconductors. The most important difference between solar cells based on inorganic and organic semiconductors is that in inorganic solar cells, photons are directly converted into free charge carriers. Then, the charge carriers can be collected by the corresponding electrodes. However, an organic photovoltaic device operation involves the following fundamental steps.

(i) Exciton Generation

Light is primarily absorbed in the conjugated polymer of the active material, which leads to the creation of excitons, or generally, absorption leads to formation of strongly bound singlet (spinless) excitons. In organic BHJ solar cells, the absorption of incident light mainly takes place in the donor material, i.e., in the conjugated polymer domains. The main limit for the photon absorption is the bandgap in the polymer. Only incident light with energy larger than the bandgap is absorbed within the active material. The photon absorption also varies with absorption coefficient and thickness of the active area. Another loss is the reflection of photons at the surface of the solar cell, which stops the photons before reaching the active material **[**25**].**

(ii) Exciton Diffusion

In order to be separated, the exciton has to diffuse towards the donor-acceptor interface within its lifetime. If the exciton does not reach the donor acceptor interface it will recombine, and the absorbed energy is converted into thermal energy or as an emitted photon and cannot be used for power generation. If the exciton reaches the interface, it

can dissociate with the electron transferring to the acceptor material leaving hole on the donor material [25].

(iii) Exciton Dissociation

The binding energy of the exciton is not well defined due to the disorder present in conjugated polymers. But a typical value is 0 - 4 eV and room temperature is not sufficient enough to dissociate the exciton [33]. As already mentioned, the considerable binding energy of these neutral excitations demands an electronegative acceptor material for exciton splitting. The charge transfer happens in the interface between the donor and acceptor material due to the difference in ionization potential and electron affinity between the materials. Consequently, charge transfer in polymer films is critically determined by the degree of interchain overlap or chain packing [34]. Well-packed chain geometries give well-ordered crystalline phases that enhance electron delocalization length and, therefore, lead to high charge carrier mobility. After charge transfer a bound charge pair is formed with a hole in the donor, and bound to an electron in the acceptor, this is sometimes called the charge transfer state **[**35]. From the charge transfer state the bound charge pair can either decay to the ground state or separate into free charge carriers. The probability of charge separation is dependent on temperature, field, diffusion length of the excitons and LUMO levels of the donor and acceptor. Figure 2.10 shows charge transfer in polymer-fullerene solar cell**.**

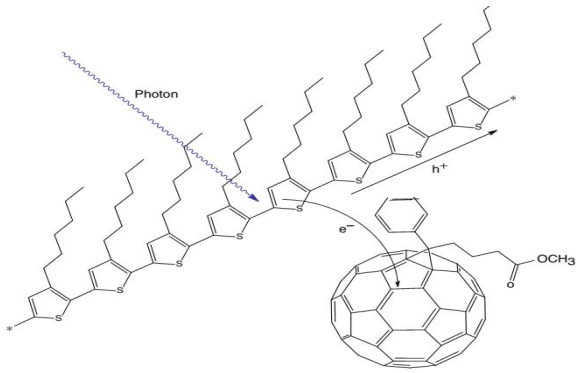

Figure 2.10: Charge transfer in a polymer-fullerene solar cell.

(iv) Charge Carrier Transport

After the dissociation of the exitons, the generated charge carriers have to be transported to the electrodes. An efficient charge carrier transport to the electrodes requires an interpenetrating network with bicontinuous percolated pathways formed from donor and acceptor phases. However, interaction with atoms and other charges may slow down the travel speed of the charge carriers and result in further recombination [36]. Figure 2.11 shows charge transport in polymer-fullerene solar cell i.e. transportation of positive holes though the conjugated polymer where as electrons along the acceptor fullerenes chain. Electron mobility in fullerenes is typically high enough to allow nearly 100% efficient extractions of electron to the cathode.

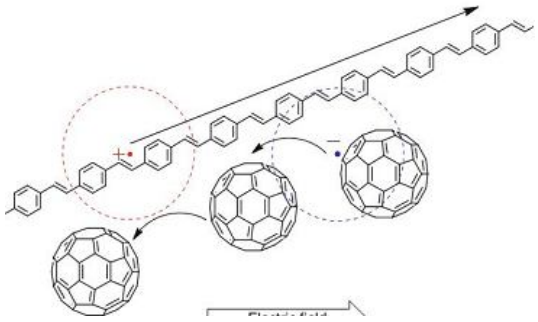

Figure 2.11: Charge transport in a polymer-fullerene solar cell.

(v) Charge Carrier Extraction

Charge carriers, which do not recombine or get caught in deep traps during their transport, can finally be extracted at the contacts. In order to contribute to the photocurrent, electrons have to leave the device *via* the cathode whereas holes have to be extracted through the anode. The generated photocurrent has a major impact on the characteristics of an organic solar cell. Figure 2.12 shows fundamental steps in organic solar cell during operation.

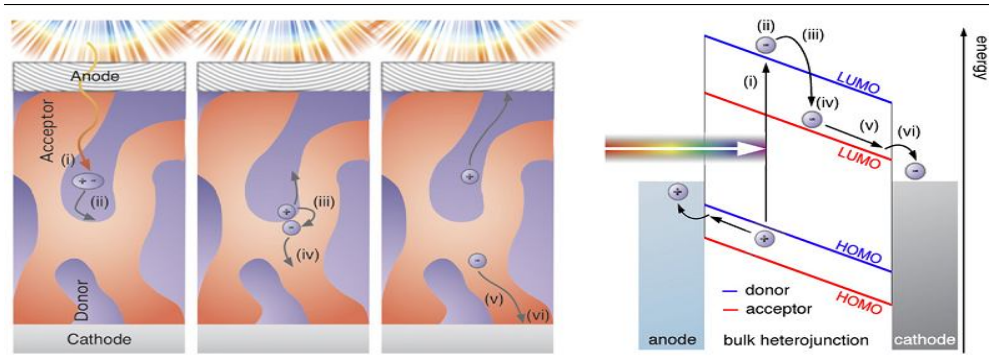

(a) (b)

Figure 2.12: Diagrammatic representation of photocurrent generation in organic BHJ solar cells starting from (a) kinetic point of view (b) simplified energy diagram.

Where (i) singlet exciton generation from an absorbed photon in the donor material, (ii) exciton diffusion to the acceptor interface, (iii) exciton dissociation by electron transfer to the electronegative acceptor molecules (iv), (v) charge transport and (vi) extraction of the charges, to give photocurrent.

2.5 Characterization of Organic BHJ Solar Cells

2.5.1 The Current Density-Voltage (J-V) Characteristics

Typical polymer/acceptor BHJ solar cell current-voltage (J-V) characteristics measured in the dark and under white light illumination conditions are depicted in Figure 2.13. The J-V curve measured under 100 mW/cm^2 sun illumination immediately gives several photovoltaic parameters such as open-circuit voltage (V_{oc}), short-circuit current density (J_{sc}), fill-factor (FF), maximum power point (MPP), and overall power conversion efficiency (η) [37]. Each of these important polymer solar cell parameters are shortly described below.

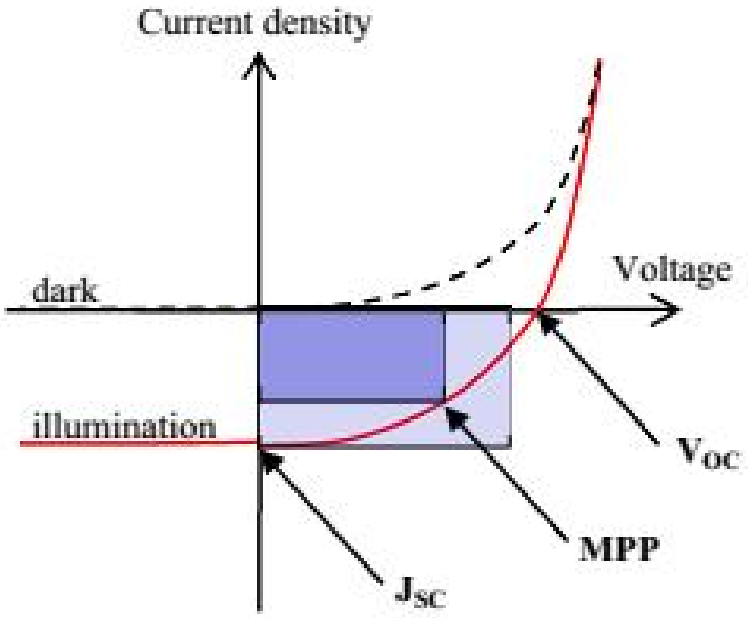

Figure 2.13: A typical J-V characteristic of a solar cell with device parameters.

i. Open-Circuit Voltage (V_{oc})

The open-circuit voltage (V_{oc}) is defined as the voltage between the two terminals of a device when there is no external load or it is the maximum voltage that can be generated by the device and measured when there is no current passing through the cell. Therefore, it is the x- intercept of the J-V curve. In organic BHJ solar cells V_{oc} can be determined from the energy difference between the HOMO energy of the donor and the LUMO energy of the acceptor. For the ideal diode, the V_{oc} increases logarithmically with light intensity and is given by:

$$V_{oc} = \frac{nkT}{q} ln(\frac{J_{sc}}{J_o} + 1) \quad \text{.....(1)}$$

Where n is the diode ideality factor (typically between 1 and 2), J_o is the saturation current density of the diode (caused by diffusion of minority carriers from the neutral region to the depletion region), q is the elementary charge, 1.6 x 10^{-19} C, k is Boltzman constant of value 1.38 x 10^{-23} J/K, T is the Kelvin temperature of the cell and J_{sc} is light generated current density [38].

ii. Short-Circuit Current Density (J_{sc})

Short-circuit current density (J_{sc}) is the photogenerated current (current density) of a solar cell, which is extracted at zero applied voltage or no external resistance between anode and cathode. i.e. it is determined in the condition when the voltage (V) across the cell is set to zero, under illumination of the cell. Photocurrent is directly related to optical and electrical material properties.

iii. Maximum Power Point (MPP)

This is another characteristic point in the 4th (power-generating) quadrant of the J-V curve. MPP is the product of maximum current and voltage (as labeled in Figure 2.13), and it can be calculated by

$$MPP = J_{max} * V_{max} \quad \text{.....(2)}$$

Where MPP is maximum power point, J_{max} is maximum current density and V_{max} is maximum voltage [39].

iv. Fill Factor (FF)

FF is a key quantity used to measure solar cell performance. Compared to V_{oc} and J_{sc}, the FF is much more sensitive to quality of device. The fill factor is given by the quotient of maximum power measured (dark blue rectangle) and the theoretical power (Aqua rectangle) as shown in Figure 2.13. It therefore describes the 'squareness' of the solar cell's current density-voltage characteristics. The equation for factor (FF) is given by

$$FF = \frac{J_{max} * V_{max}}{J_{sc} * V_{oc}} \quad \text{.....(3)}$$

Where J_{max}, V_{max}, J_{sc}, and V_{oc} are maximum current density, maximum voltage short-current density, and open-circuit voltage respectively.

A high fill factor is advantageous and indicates that fairly strong photocurrents can be extracted from the device. A high fill factor can be obtained when the charge mobility of both charges (electron and hole) is high. In general, it depends on the mobility-lifetime product of charges in the active material, the thickness of the active layer, as well as the

morphology of the active layer. Moreover, a big series resistance would also lower the FF in BHJ based organic solar cells [40].

v. Power Conversion Efficiency (η)

The single most important performance parameter of a solar cell is the power conversion efficiency (η), which is related with the open-circuit voltage (V_{oc}), short-circuit current (J_{sc}) and fill factor (FF) through Equation (4). All of those parameters can be extracted from the J-V curves under the 1 sun condition (100 mW/cm^2, simulated AM 1.5G solar illumination). The power conversion efficiency PCE is the most important parameter for solar cells as it indicates how cell is efficient. The power conversion efficiency (η) is simply the ultimate measure of the device efficiency in converting photons to electrons. It is defined as the power output divided by the incident light power. Mathematically it is calculated using equation (4) [41].

$$\eta(\%) = \frac{P_{out}}{P_{in}} * 100 = \frac{FF * J_{sc} * V_{oc}}{P_{in}} * 100 \quad \text{.....(4)}$$

Where P_{in} is the power density of the incident light (100 mW/cm^2) and P_{out} is the electric power generated by the cell at the maximum power point.

2.5.2 Spectral Response

J-V characteristic of a solar cell recorded under the illumination of white light does not provide detailed information on the spectral coverage and the efficiency of the device that convert monochromatic light into electricity. The short-circuit current generated at every wavelength defines the spectral response S_i of the solar cell, which is defined as:

$$S_i = \frac{J_{sc,i}}{P_{in,i}} \quad \text{.....(5)}$$

Where $J_{sc,i}$ is the photogenerated short-circuit current at a specific excitation wavelength λ_i and $P_{in,i}$ is the incident monochromatic photon intensity. S_i is directly correlated to the external quantum efficiency (EQE) of a solar cell [42].

EQE is sometimes referred to as an incident photon to current conversion efficiency (IPCE). Experimentally, EQE is measured without taking care of optical loses such as light transmission through the cell and reflection away from the cell. Effective carrier generation after correction for optical loses is characterized by the so-called internal quantum efficiency (IQE). Incident photon-to-current conversion efficiency (IPCE) also called external quantum efficiency is the ratio of the number of collected charge carriers to the number of incident photons. This is an important parameter to determine the quantum efficiency of a device as a function of the energy or wavelength of the incident radiation. For a particular wavelength, it specifically relates the number of charge carriers collected to the number of photons shining on the device. Quantum efficiency alone is not the same as overall energy conversion efficiency, as it does not convey information about the fraction of power that is converted by the solar cell.

$$IPCE(\%) = \frac{E_{ph}(\lambda) * J_{sc}}{P_{in} * e} = \frac{1240 * J_{sc}}{\lambda * P_{in}} \quad \text{.....(6)}$$

Where E_{ph} (λ) is the energy of a photon (Joule), e is the electronic charge, J_{sc} is short-circuit current density ($\mu A/cm^2$), λ is the excitation wavelength (nm) and P_{in} is the incident photon intensity (W/m^2) at each wave length. The ratio, E_{ph}/P_{in}, refers to the number of incident photons while; J_{sc}/e refers to the number of electrons that generate electricity and $1240/\lambda$ refers to the energy of photons in eV [43].

2.6 Efficiency Limiting Factors in Organic BHJ Solar Cells

Power conversion efficiency of a BHJ based organic solar cells are directly correlated to the three key parameters, namely J_{sc}, V_{oc}, and FF. This means η is inherently related to material properties, device structure and interface effects.

The photocurrent (J_{sc}) of polymer solar cells is affected by several factors including light intensity, light absorption rate (spectral mismatch), exciton generation and dissociation rate, and the carrier transport in the active layer etc. The absorption of light or exciton generation rate depends on the active layer thickness and the bandgap of the active materials. The exciton dissociation rate mainly depends on the interfacial area between donor and acceptor, and in BHJ films the dissociation rate is quite efficient due to the availability of polymer/acceptor junctions within the range of exciton diffusion length. Molecules with high electron affinity, such as the fullerene [6,6]-phenyl-C_{61}-butyric acid methyl ester ($PC_{61}BM$), are usually employed as the acceptor for organic solar cells [44] in order to rapid exciton dissociation and get efficient power conversion efficiency. The polymer/C_{60} interpenetrating networks give ultra fast (less than 100 fs) [45] electron

transfer rate from the optically excited polymer to C_{60} molecule. This time regime is so small that competing decay processes are extremely minimized leading to an almost complete (100%) charge transfer processes**.** Thus, the efficiency of organic BHJ based solar cells is not greatly affected by exciton dissociation rates but it is rather limited by the exciton generation rate and collection efficiency of free charge carriers as compare to other organic photovoltaic methods.

The optical absorption of most conducting polymers covers the visible range of the solar spectrum up to 700 nm to construct efficient solar cells [46]. Moreover, to enhance the optical absorption in solar cell materials two mechanisms are mandatory. The first option is utilizing long wavelength photons that can be realized by using low bandgap polymers. The second option is utilizing an appropriate thickness of films in order to harvest photons in wide range of the solar spectrum. Therefore, to draw substantial photocurrent from organic BHJ based solar cells, well-designed polymers that render broad optical absorption band and form well ordered chains should be considered as the best choice.

The second photovoltaic parameter that limits efficiency is the open-circuit voltage. The V_{oc} of organic BHJ based PSCs mainly originates from the electronic levels of the donor polymer and the acceptor molecule. In general, V_{oc} is limited by several factors including interfacial energy levels, shunt losses and morphology of the active film [47]. For organic BHJ solar cells with ohmic contacts, V_{oc} is mainly determined by the difference between the HOMO of the donor polymer and the LUMO of the acceptor molecule indicating how much the electronic levels are crucial in determining the efficiency of such solar cells.

The third important parameter that limits efficiency is a fill factor. The direct relation of FF with current density indicates (Equation 3) that it is greatly affected by the mobility of the charge carriers. Moreover, series resistance is also one of the limiting factor of fill fctor in organic BHJ based PSCs [48]. In general, a large series resistance, small shunt resistance, and recombination tend to reduce the FF.

2.7 Methods to Control the Morphology of Organic BHJ Solar Cells

Active layer morphology control is of paramount importance for the performance of organic bulk heterojunction (BHJ) solar cells. Charge-carrier formation in organic solar cells takes place only at the interface between the donor and acceptor compounds. Therefore, only photons that are absorbed within the exciton diffusion length from the interface can contribute to the device photocurrent. Electron and hole transport occurs by hopping through the acceptor and donor phases, respectively. Consequently, the morphology of organic BHJ solar cell, which is comprised of an interpenetrating bicontinuous network, must assure a large interface between both phases, as well as continuous pathways to both electrodes [49].

i. Thermal Annealing

Historically, thermal annealing of the film has been used to induce optimum phase separation between donor and acceptor in bulk heterojunction blends. However, thermal treatment creates an additional fabrication step in the whole device fabrication process. Later, various methods have been tested and employed to control the nanomorphology of the blends, namely use of solvents with different boiling points (choice of host solvent), reduction of drying speed (rate of drying) and changing the solubility of materials, and

the use of processing additives (chemical or solvent). The later method has got great interest as it removes the need for post-production treatment while at the same time allowing fine control of the nanomorphology in various donor-acceptor blends. Use of processing additives is an attractive concept due to the simplicity and suitability for large-scale production [50].

ii. Processing Solvents

One advantage of PSCs is that they can be fabricated *via* solution process. The solubility of polymers varies in different organic solvents**.** Therefore, the interaction between donor polymer and acceptor ($PC_{61}BM$) in solution or during the film drying process will be different when different solvents are used which could result in different active layer morphologies [51]. Hence, choice of processing solvent is a key step in fabrication of polymer solar cells.

iii. Donor-Acceptor Ratio

The donor (D) and acceptor (A) blend ratios significantly influence the device performance of the organic BHJ solar cell. It has been shown that the D-A ratio greatly influences the performance of the organic BHJ solar cell as it strongly affects the crystalline order, phase separation, and morphology of the thin film form bicontinuous percolation pathways with maximal interfacial area [52]. The optimal D-A ratio depends on the choice of materials used.

iv. Solvent Additive Effect (Polar Solvent)

Despite to the thermal annealing, processing solvents and blending ratio, overall performance can be significantly enhanced by treatment of organic BHJ active layer with polar solvents during solution processing before deposition of metal electrodes. However, there are two general convectional guidelines during selection of solvent additives. (1) One active layer component must be significantly more soluble in the solvent additive than the other component mainly to the fullerene component. When a single solvent that is good for the two components of the organic BHJ blend is used, the chains remain solvated up to a point where viscosity inhibits their motion and they are unable to attain similar packing characteristics [53]. (2) The boiling point of the solvent additive must be significantly greater than that of the processing solvent to maximize the interaction time between the additive and the active layer components during thin film formation [54]. Because of their higher boiling point, the solvent additives evaporate more slowly than the host solvent does. Figure 2.14 is schematic representation that shows how solvent additive affects morphology of BHJ based organic solar cells.

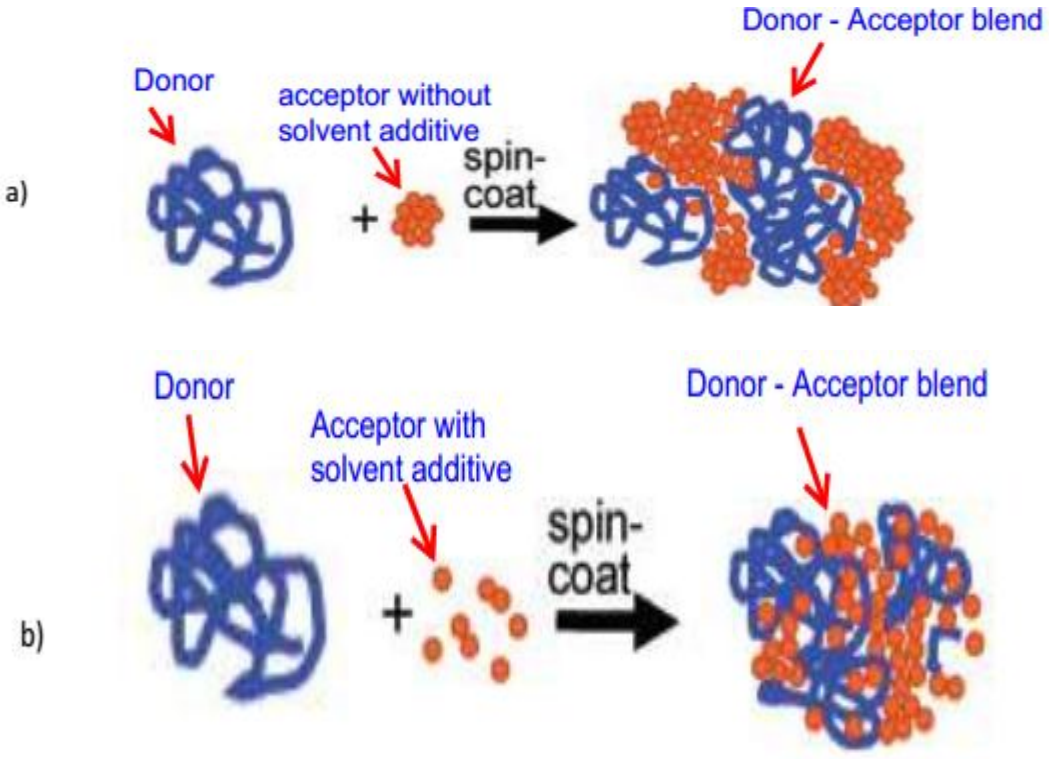

Figure 2.14: Schematic diagrams showing the effect of solvent additive a) morphology processed without solvent additive (SA) b) with solvent additive.

3. OBJECTIVES

3.1 General Objective

- To study the effect of low boiling point solvent additives (iodomethane, iodoethane and di-iodomethane) on photovoltaic performance of TQ1**:**$PC_{61}BM$ based bulk heterojunction solar cells.

3.2 Specific Objectives

- To construct organic BHJ solar cells based on TQ1:$PC_{61}BM$ containing each of the solvent additives
- To characterize the organic BHJ solar cells using various standard characterization techniques such as J-V and IPCE
- To optimize the composition of each solvent additives on the performance of the fabricated organic BHJ solar cells
- To look into the effect of each additives on the blend using UV-Vis and photoluminescence (PL) spectrophotometers
- To compare the relative effect of each solvent additives on performance of the organic BHJ solar cells

4. EXPERIMENTAL DETAILS

This chapter introduces the materials used and procedure of organic BHJ solar cell devices fabrication.

4.1 Instruments and Apparatus Used

Instruments and apparatuse used in this study were: Ultrasonic bath for cleaning the ITO coated glass substrates and vials, UV-Vis spectrophotometer (Lambda9-UV/Vis/NIR, PerkinElmer, USA) for measuring the optical absorption spectra of solution and thin film samples, Spectrofluometer (FluoroMax-4, Jobin Yvon, USA) for measuring photoluminesence intensity of solution and films, Spin-coater (KW-4A) for PEDOT-PSS and active layer film formation, Vacuum evaporator (Edward-306) for depositing Al as cathode electrode, Electrochemical Analyzer (CHI630A) for measuring J-V, Tungsten-halogen lamp together with power source (68830-Oriel) as light soures for measuring the J-V characteristic and IPCE of the cells, Monochromator (Model 77250) as a wavelength ssselector, and Gigahertz-Optik (X11-Optometer) for adjusting the intensity of light to the standard value, and weighing balance (Denver instrument XE-50) for weighing solid chemicals.

4.2 Materials, Chemicals and Reagents

■ ITO Coated Glass Substrate

Indium tin oxide (ITO) is a transparent conductive oxide which is used as anode. Figure 4.1 shows the schematic sketch of pre-patterned ITO coated glass used in this work. Its work function is 4.7 eV [55].

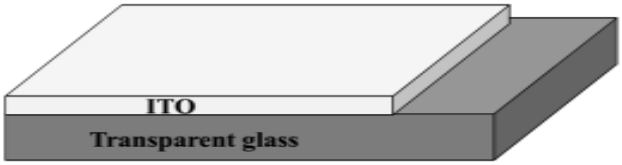

Figure 4.1: Structure of pre-patterned ITO coated glass used.

- **PEDOT-PSS** (Sigma-Aldrich)

Poly(3,4-ethylenedioxythiophene-Poly(4-styrenesulfonate) [PEDOT-PSS] is conducting conjugated polymer (Figure 4.2) which is used as hole transporting layer. The work function of PEDOT-PSS is ~5.2 eV [56].

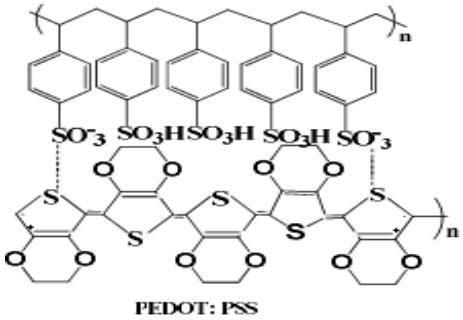

Figure 4.2: Molecular structure of PEDOT-PSS.

- **TQ1 polymer** (Synthesized at Chalmers University, Sweden)

Poly[2,3-bis-(3-octyloxyphenyl)quinoxaline-5,8-diyl-alt-thiophene-2,5-diyl] (TQ1) is very strong electron donor conjugated polymer [57] (Figure 4.3). Hence, it is used as light absorbing material. Its optical bandgap is around 1.7 eV [58].

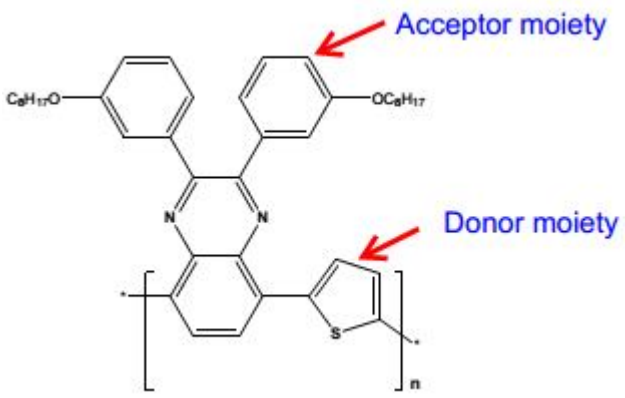

Figure 4.3: Molecular structure of TQ1 polymer.

- **$PC_{61}BM$** (Sigma-Aldrich)

Phenyl-C_{61}-butyric acid methyl ester ($PC_{61}BM$) is a fullerene-based molecule (Figure 4.4) used as an electron acceptor in the bulk heterojunction solar cell devices studied. It contains a Bucky-ball (C_{60}), and to make it soluble the methyl-ester group is attached. Its HOMO and LUMO level are 6.1 eV and 3.7eV, respectivelly [59]**.** $PC_{61}BM$ is highly soluble in chlorobenzene, toluene, chloroform and similar organic solvents.

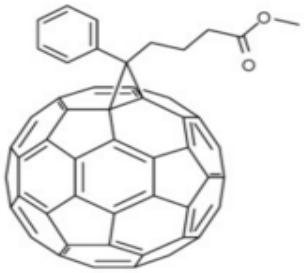

Figure 4.4: Molecular structure of $PC_{61}BM$ polymer.

- **Solvents**

The different solvents used in this work are: distilled water, isopropanol, acetone, chloroform as cleaning solvents (Sigma - Aldrich), iodomethane, iodoethane and di-

iodomethane as solvent additives (BDH chemicals Ltd Poole England), and o-dichlorobenzene as host solvent (Riedel–de Haen, UN). Figure 4.5 shows the chemical structure and Table 4.1 shows the physical properties of the solvent additives and host solvent.

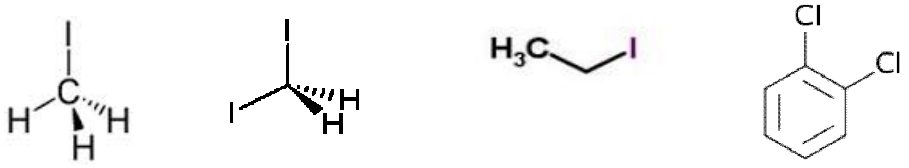

(a) (b) (c) (d)

Figure 4.5: Molecular structure of organic solvents used in solar cells a) iodomethane b) di-iodomethane c) iodoethane and d) o-dichlorobenzene.

Table 4.1: Physical properties of the host solvent and solvent additives used.

Solvents	Molecular Weight (g/mol)	Boiling Point (^{o}C)	Dielectric Constant (F/m)
Iodomethane (IMe)	142	42	7.0
Iodoethane (IEt)	156	72	7.4
Di-iodomethane (DIMe	268	181	8.9
o-dichlorobenzene (o-DCB)	146	178	9.9

- **Aluminum and Silver Paste** (Agar Scientific, Essex, England)

Pieces of Al rod were evaporated on the top of active material using the vacuum evaporator to be used as cathode electrode in this work. The advantage of using Al metal is because of its low melting point and availability. Its work function is 4.3 eV [60].

Silver-paste in this study was used for contact to avoid easily scratching of the Al electrode during characterization.

4.3 Procedure of Organic BHJ Solar Cell Devices Fabrication

4.3.1 Solution Preparation

A 1:2 (w/w) ratio of TQ1:$PC_{61}BM$ solution (25 mg/mL) [61] was prepared by mixing 1 mg of TQ1 and 2 mg of $PC_{61}BM$ in 120 μL of nitrogen-cleaned solvent (o-dichlorobenzene) in a cleaned brown vial. With the same procedural condition, 3% (v/v) solvent additives (IMe, IEt and DIMe) of o-DCB were added to other three vials and blend solutions with concentation of 25 mg/mL were also prepared. Then, cleaned magnetic stirrer was introduced into solution for stirring to enhance solubility and miscibility of the blends. Finally, the solution were left overnight under stirring at 80^{o}C hot plate to obtain a homogeneous solution.

4.3.2 Optimization of Solvent Additives

Optimization on the percent composition (v/v) of solvent additives was done using iodomethane, iodoethane and di-iodomethane independently. TQ1:$PC_{61}BM$ samples processed in o-dichlorobenzene (pristine) and o-dichlorobenzene containing 3%, and 4% (v/v) of each solvent additives were prepared. Then films of each sample solutions were prepared for bulk heterojunction solar cells optimization and characterization.

4.3.3 Device Fabrication

For absorption and PL experiments, thin films were prepared by spin coating the active layer (TQ1:$PC_{61}BM$ in optimal 1:2 ratio (w/w) dissolved in o-DCB, o-DCB wih solvent additives) on a transparent glass slides.

For J-V measurement device fabrication, the pre-patterned ITO glass substrates with a sheet resistance of 15 Ω/cm^2 were washed manually in detergent, acetone and isopropan56ol, and also ultrasonically by distilled water, acetone and isopropanol sequentially for 15 min. Prior to use, the substrates were dried with an air gun. A filtered dispersion of aqueous solution PEDOT-PSS was then spin coated onto cleaned ITO substrates at 3500 RPM for 60 seconds and then baked at 130°C hot plate for 15 min. Then, deposition of the active layer (TQ1:$PC_{61}BM$ in 1:2 (w/w), 25 mg/mL (optimum)) was spin coated at 1000 RPM spin speed for 60 seconds on the top of PEDOT:PSS layer using spin coater.

The devices were completed for measurement after thermal deposition of aluminum film (as the cathode) on the top of the active layer by thermal evaporation in vacuum with a thickness of ~99 nm in three solar cells leaving mask. The thickness was measured using a well-calibrated quartz crystal thickness monitor. The vacuum pressure was under $\sim 5\times10^{-6}$ mbar, and the deposition rate of aluminium was controlled at ~3 - 5 nm/s. Silver-paste paint was made at the contact of each electrode just to avoid easy scraching of the Al electrode during characterization. The area of these fabricated devices were 6 mm^2. Finally, the formed glass/ITO/PEDOT-PSS/TQ1:$PC_{61}BM$/Al (~99 nm) BHJ photoactive device characterizations were carried out under AM 1.5G irradiation from Tungsten-

halogen lamp (250 W) with the intensity of 100 mW/cm^2 from power source. Figure 4.6 shows the schematic representation for device preparation steps of the organic BHJ solar cells used in this work.

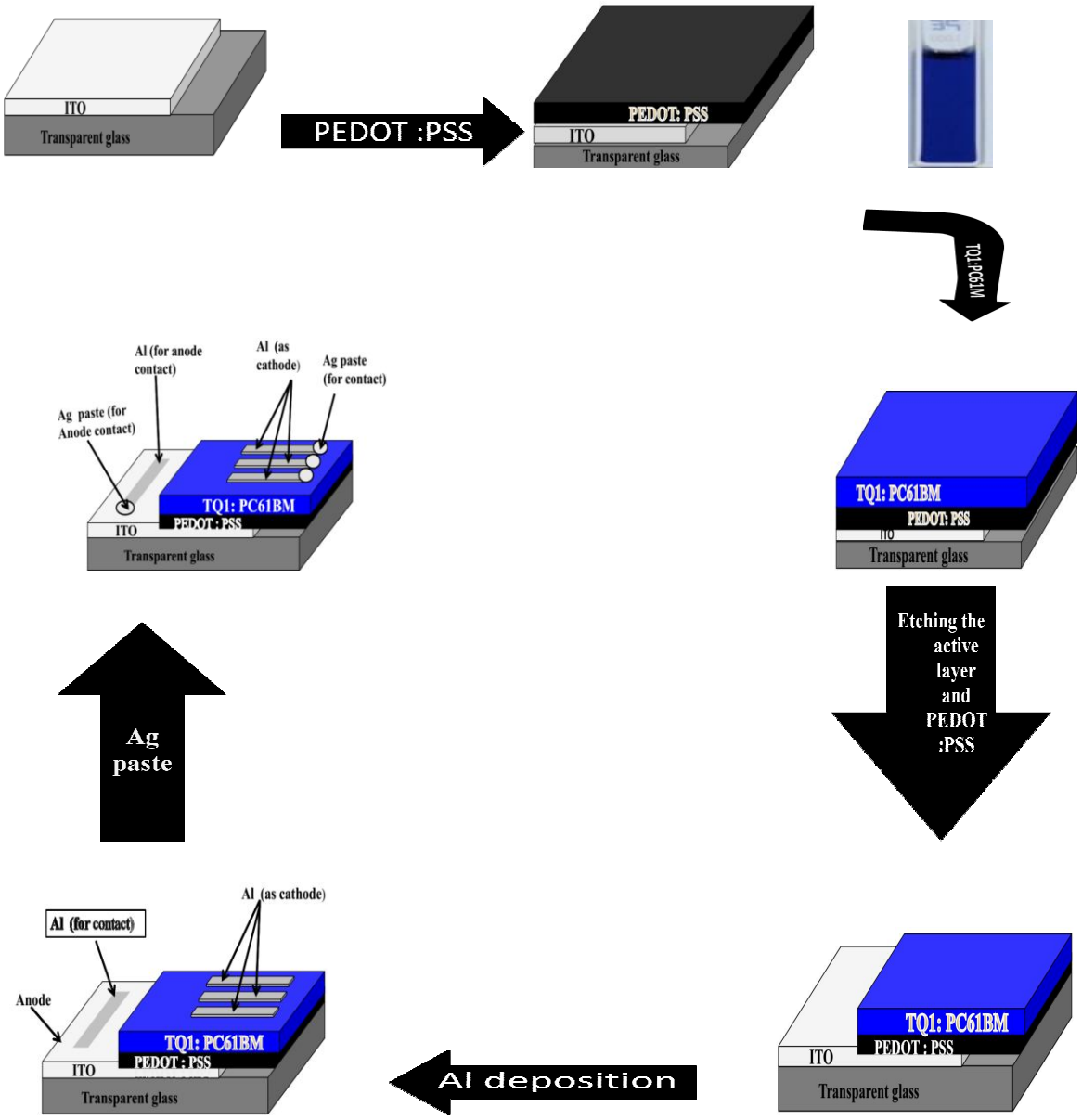

Figure 4.6: Schematic representation for device preparation steps of glass/ITO/PEDOT-PSS/TQ1:PC61BM/Al (~99 nm) BHJ solar cells.

4.4 Experimental Methods

- Absorption spectra of films on transparent glass were measured against the transparent glass substrate as a blank and thin film absorption spectra were recorded using UV-Vis Spectrophotometer (Lambda9-UV/Vis/NIR, PerkinElmer, USA) from 300 nm to 800 nm wavelength range.
- The photoluminescence intensity of each fabricated films were measured using spectrofluometer (FluoroMax-4, Jobin Yvon, USA).
- The J-V measurements of the cell was performed using a computer-controlled CHI630A Electrochemical Analyzer, and a 250 W Tungsten–halogen lamp regulated by an Oriel power supply (Model 68830) was used to illuminate the organic BHJ solar cells. Before illumination the device, the white light intensity was set to 100 mW/cm^2 using Gigahertz-Optik X11 Optometer.
- For IPCE, a grating monochromator (Model 77250) placed into the light path, which was used to select a wavelength between 300 and 800 nm. The photocurrent spectral response of the lamp was corrected using a standard silicon photodiode (Hamamatsu, Model S1336-8BK).

5. RESULT AND DISCUSSION

5.1 UV-Visible Absorption

The UV-Vs absorption spectra were investigated both from solution and film on transparent glass of pristine polymer and the blend of the polymer with $PC_{61}BM$. The absorption spectrum of pristine TQ1, both in solution and film, shows two distinct peaks (Figure 5.1a). Table 5.1 shows the absorption maxima of TQ1 and TQ1:$PC_{61}BM$ both in solution and thin films. The absorption peak at longer wavelength is due to charge transfer between the acceptor moiety and donor moiety of TQ1, as the polymer is made of donor-acceptor (D-A) repeating unit (Figure 4.3); where as the absorption peak corresponding to the shorter wavelength is due to the $\pi - \pi^*$ transition. Figure 5.1a also compares the UV-Vis spectra of pristine polymer both in solution and film. As shown in the Figure, absorption maximum in the visible region for TQ1 in solution and film occurred at 601 nm and 624 nm, respectively, indicating that the absorption of the film was red-shifted compared to that of the solution due to the aggregation of the polymer chains and an orderly $\pi - \pi^*$ stacking formed in the solid state fastening charge transfer between D-A moieties of the polymer [62]. In the same manner, the absorption peak position of the pristine TQ1 film at shorter wavelength is also red-shifted (365 nm) compared to its corresponding solution phase (356 nm) confirming the agreggation of the polymer and ordering of the $\pi - \pi$ stacking. This also facilitates the $\pi - \pi^*$ transition by extending the conjugation length that in turn narrows the bansdgap. From the spectrum features of pure TQ1:$PC_{61}BM$ film (Figure 5.1b (2)), two absorption peaks at 338 nm and 625 nm are also observed. The absorption peak at shorter wavelength (338 nm), even

below that of the pristine TQ1 (365 nm), is due to the absorption of $PC_{61}BM$ and the peak at the longer wavelength (625 nm), which is consistent with pristine TQ1 film absorption peak (624 nm), is absorption contributed from the polymer. Another feature which can be observed from the absorption spectra of the blend is that addition of $PC_{61}BM$ to the polymer fills the large absorption valley observed between 375 nm and 575 nm in the spectra of pristine TQ1 polymer. This in one or the other way contribute to harvesting large amount of incident photons that may contribute to the enhancement of photocurrent of the solar cell. Generally, for the absorption spectra of many conjugated polymers, there is a red-shift that occurs when it goes from the solution to the solid state due to the aggregation of the polymer chains in the solid state.

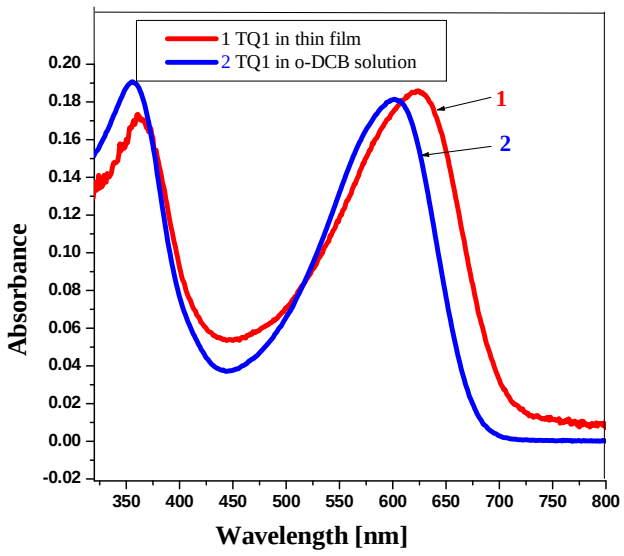

(a)

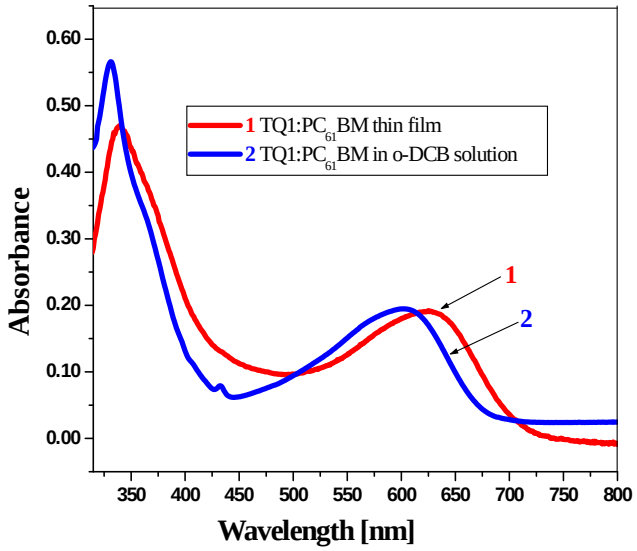

(b)

Figure 5.1: Absorption spectra of a) TQ1 in o-DCB solution (2) and film (1), b) TQ1:$PC_{61}BM$ in o-DCB in solution (2) and film (1).

Table 5.1: λ_{max}, absorption of TQ1 and TQ1:$PC_{61}BM$ in o-DCB solution and thin films.

Sample	UV-Vis	
	λ_{max1}, abs (nm)	λ_{max2}, abs (nm)
TQ1 in o-DCB solution	356	601
TQ1 film	365	624
TQ1:$PC_{61}BM$ in o-DCB solution	331	602
TQ1:$PC_{61}BM$ film	338	625

Figure 5.2 shows UV-Vis spectra of TQ1 and TQ1:$PC_{61}BM$ (pristine) films spin coated from blend solutions containing 3% (v/v) of low boiling point solvent additives; iodomethane, iodoethane, and di-iodomethane. As it can be observed from the spectra and table 5.2, addition of these solvent additives has not affected the absorption feature significantly, i.e. absorption peak positions at both short and long wavelengths compares to the pristine blend of TQ1:$PC_{61}BM$. However, among the low boiling point additives, the incorporation of the DIMe slightly affected the absorption of the films from the pristine blend and caused minor red-shift in the λ_{max} value. This observed slight red-shift by incorporation of di-iodomethane is due to more effective packing of chains in the polymer. But the spectra of films obtained from blend solution containinig these additives revealed broad absorbance over the entire visible region up to approximately 700 nm similar to the pristine blend. Furthermore, blend films with these solvent additives show stronger absorption peaks within the range of 300 - 800 nm compared to the pristine blend film. The stronger absorption could be ascribed to the more ordered structure of TQ1 with the treatment of additives, and it should be beneficial to the increase of J_{sc} and PCE values. Importantly, in the presence of solvent additives, $PC_{61}BM$ aggregates will dissolve and well segregate throughout the polymer chain. This will cause the polymer

chains to redistribute that results in the growth of enhanced local structure with improved crystalline and order of TQ1 domain [63].

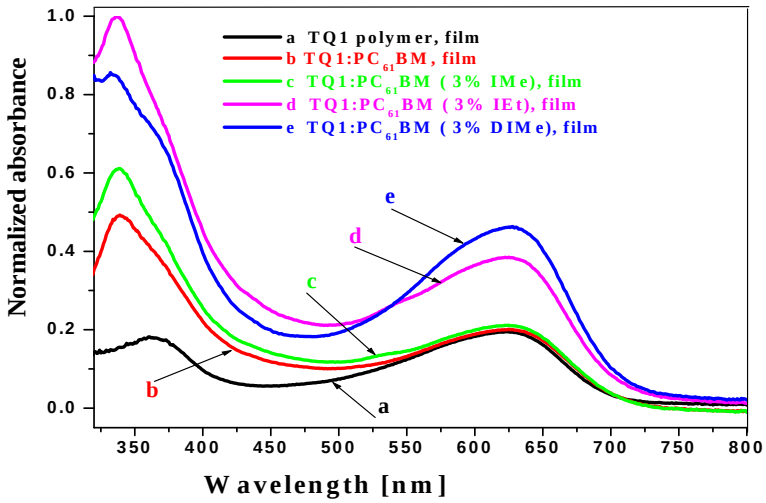

Figure 5.2: Normalized absorption spectra of a) TQ1 b) TQ1:$PC_{61}BM$ (0%), c) TQ1:PC61BM (3% IMe), d) TQ1:PC61BM (3% IEt), e) TQ1:PC61BM (3% DIMe) films, spin coated on transparent glass slides at 1000 RPM processed from 5 mg/mL solution in pure o-DCB.

Table 5.2: λ_{max}, absorption of TQ1, TQ1:$PC_{61}BM$ (pristine), TQ1:$PC_{61}BM$ (3% IMe), TQ1:$PC_{61}BM$ (3% IEt) and TQ1:$PC_{61}BM$ (3% DIMe) films.

Sample (film)	UV-Vis	
	λ_{max1}, abs (nm)	λ_{max2}, abs (nm)
TQ1	365	624
TQ1:$PC_{61}BM$ (Pristine)	338	625
TQ1:$PC_{61}BM$ (3% IMe)	338	624
TQ1:$PC_{61}BM$ (3% IEt)	336	625
TQ1:$PC_{61}BM$ (3% DIMe)	332	628

5.2 Photoluminescence Spectra

Figure 5.3 shows the photoluminescence (PL) spectra of pure TQ1 and TQ1:$PC_{61}BM$ blended active layer films run using pure o-dichlorobenzene and o-dichlorobenzene containing 3% (v/v) of iodomethane, iodoethane and di-iodomethane solvent additives. Compared to pure TQ1, the PL intensity of the blends in general is considerably reduced in the wavelength range of 650 to 850 nm. Importantly, the reduction (quenching) of the PL intensity of the polymer in the blends is due to charge transfer between the donor polymer (TQ1) and the acceptor ($PC_{61}BM$). Efficient PL quenching can usually happen when the donor polymer (TQ1) and acceptor ($PC_{61}BM$) in the blend become close enough (in the range of exciton diffusion length of ~10 nm) and increase contact interface area between them. This decreasing in fluorescence intensity may be observed due to good phase separation with improved ordered and crystalline domain of TQ1 in the blend film [64]. On the other hand, high PL intensity that is observed from PL of TQ1 film indicates that all excitons generated on TQ1 within the film are emitted more before reaching to quenching sites (defects) in the polymer film [65].

As it is also observed from Figure 5.3, the emission from a charge-transfer (CT) state is strongly quenched upon processing with IMe, IEt, and DIMe compared to pristine blend. This indicates that addition of low boiling point additives to the blend has resulted in an increment in the TQ1:$PC_{61}BM$ interfacial area. Moreover, the PL of the blend film processed from DIMe has highly quenched compared to blend films processed from IEt and IMe showing it is DIMe solvent additive that creates optimum donor-acceptor interface area and optimum morphology for efficient charge transfer and transport enhancing the photovoltaic performance of the solar cell as evidenced from Table 5.4. In

summary all blend films processed from the low boiling point solvent additives have resulted in enhancement of UV-Vis absorption (Figure 5.2) and have largely increased the PL quenching of the polymer film compared to the pristine blend processed with out additive and have resulted in increase in the photovoltaic performance of the solar cells by mainly enhancing the photocurrent (Table 5.4).

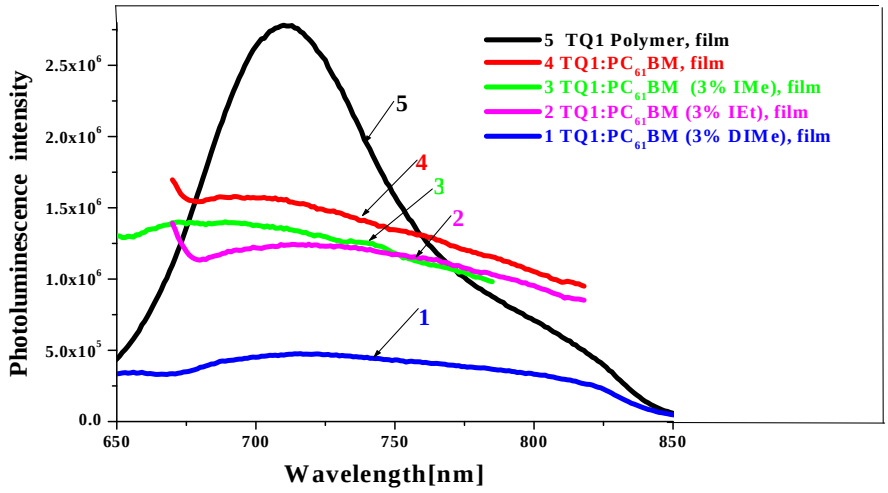

Figure 5.3: Photoluminescence spectra of TQ1 (5), TQ1:$PC_{61}BM$ composite films with various solvent additives: none (4), 3% IMe (3), 3% IEt (2), and 3% DIMe (1). The excitation wavelength is 600 nm.

Table 5.3: λ_{max}, photoluminescenc of TQ1, TQ1:$PC_{61}BM$ (pristine), TQ1:$PC_{61}BM$ (3% IMe), TQ1:$PC_{61}BM$ (3% IEt) and TQ1:$PC_{61}BM$ (3% DIMe) films.

Sample (film)	Fluorescence λ_{max}, PL (nm)
TQ1	710
TQ1:$PC_{61}BM$ (Pristine)	693
TQ1:$PC_{61}BM$ (3% IMe)	689
TQ1:$PC_{61}BM$ (3% IEt)	714
TQ1:$PC_{61}BM$ (3% DIMe)	716

Figure 5.4 shows the absorption (A) and photoluminescence spectra (B) of TQ1, TQ1:$PC_{61}BM$ (pristine) and composite films with various solvent additives.

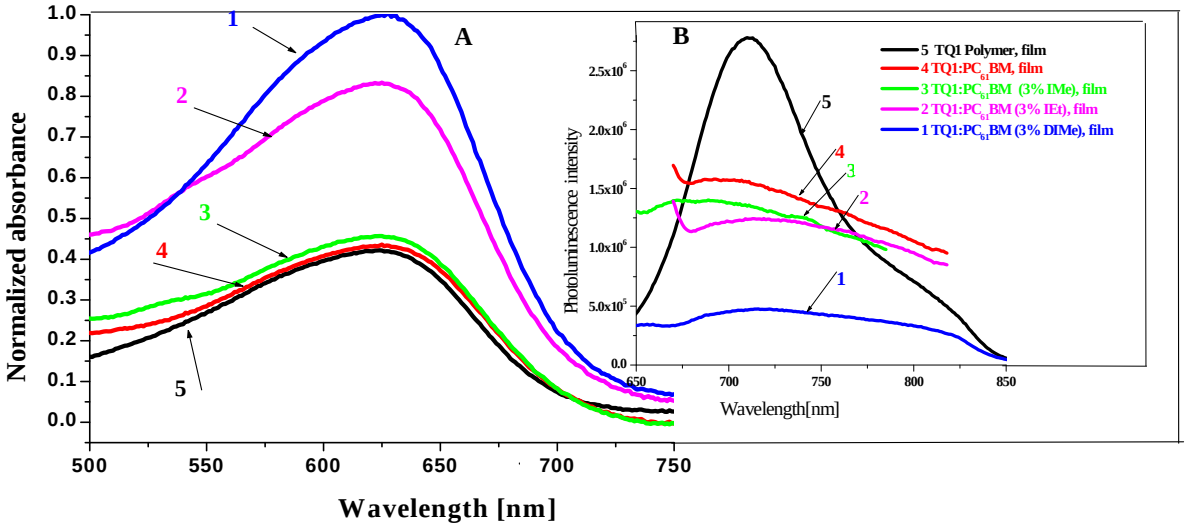

Figure 5.4: Normalized optical absorption sepectra (A), and photoluminescence spectra (B) of TQ1 (5), TQ1:$PC_{61}BM$ composite films with various solvent additives: 0% (4), 3% IMe (3), 3% IEt (2), and 3% DIMe (1).

5.3 J-V Characteristics

5.3.1 Optimization of Solvent Additives

Percent composition optimization of the low boiling point solvent additives iodomethane, iodoethane, and di-iodomethane was done independently. During the optimization, bulk heterojunction solar cells based TQ1:$PC_{61}BM$ films that are processed from o-dichlorobenzene and o-dichlorobenzene containing 3%, and 4% (v/v) of each solvent additive were fabricated. The best performing solar cell is obtained from a blend o-dichlorobenzene containing 3% (v/v) of each additive (Table 5.4). As shown from Figure

5.5 and Table 5.4, TQ1:$PC_{61}BM$ solar cell films processed from o-dichlorobenzene containing 3% (v/v) of di-iodomethane showed the best power conversion efficiency (η = 4.53%), short-circuit current (J_{sc} = 12.43 mA/cm^2), fill factor (FF = 42%) and open-circuit voltage (V_{oc} = 823 mV) as compared to its 4% (v/v), and the other solvent additives. Devices processed from iodomethane and iodoethane also showed best photovoltaic responses with (η = 3.28, 3.76%), and short-circuit current (J_{sc} = 8.41, 9.07 mA/cm^2), fill factor (FF = 47, 52%) and (V_{oc} = 808, 804 mV), respectively as compared to their corresponding 4% (v/v) additive composition. This indicates that the optimum percentage composition of all solvent additives is 3% (v/v) in o-dichlorobenzene host solvent.

As shown in Figure 5.5 (A), (B), (C) and data documented in Table 5.4, as the percent composition of the solvent additive is increased above the optimum composition of 3% (v/v), almost all photovoltaic parameters have decreased as compared to the optimum compostion, leading to poor cell performance. This might be due to the fact that increasing composition of solvent additives beyond the optimum value dissolves highly the electron acceptor ($PC_{61}BM$) and leads to extereme miscibility of the blend. This may result in poor morphology due to poor phase separation of the blend film and poor percolation of donor and acceptor materials to their corresponding electrodes which leads to more probable recombination of photogenerated charge carriers hampering the photovoltaic parametrs.

To look into the effect of solvent additives below the predicted optimum value, we prepared bulk heterojunction devices processed in o-dichlorobenzene containing 2.5% of iodobutane, which is analogous to the solvent additive used, and showed η = 2.03%, J_{sc} =

5.79 mA/cm^2, FF = 44% and V_{oc} = 792 mV. This extrem reduction in all photovoltaic parameters is arised from poor solublity of $PC_{61}BM$ in this solvent resulting in poor phase separation between TQ1and $PC_{61}BM$.

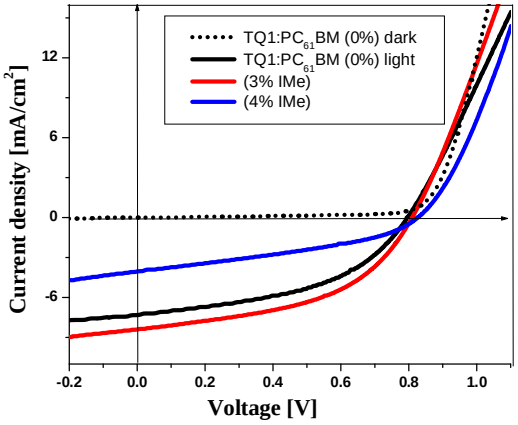

A

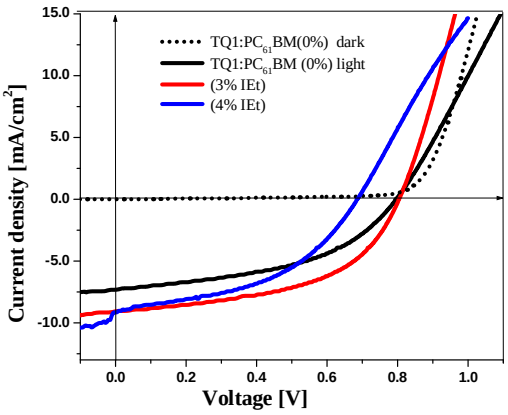

(B)

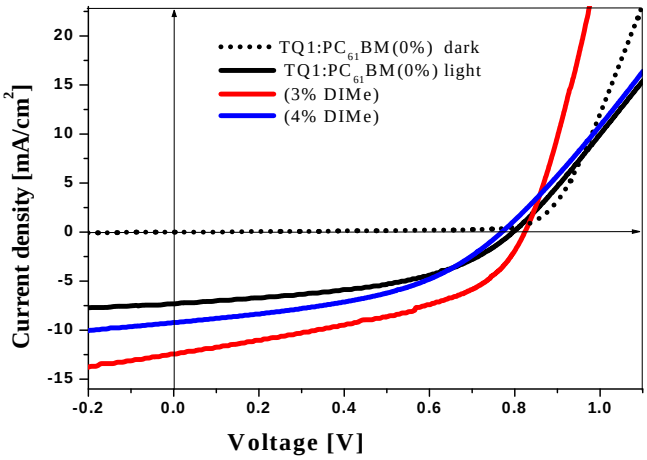

(C)

Figure 5.5: J-V curves of TQ1:$PC_{61}BM$ solar cells processed in pure o-dichlorobenzene, and o-dichlorobenzene containing 3% and 4% (v/v) of iodomethane (IMe), (A), iodoethane (IEt), (B), and di-iodomethane (DIMe), (C), solvent additives under 100 mW/cm^2, white light illumination.

Table 5.4: Photovoltaic parameters of TQ1:$PC_{61}BM$ solar cells spin-coated from o-dichlorobenzene containing 3% and 4% (v/v) of iodomethane, iodoethane and di-iodomethane solvent additives. The measurements were done at 100 mW/cm^2, white light illumination.

Conditions	V_{oc} (mV)	J_{sc} (mA/cm^2)	FF (%)	PCE (%)
TQ1:$PC_{61}BM$ (pristine)	795	7.32	47	2.71
TQ1:$PC_{61}BM$ (3% IMe)	808	8.41	46	3.28
TQ1:$PC_{61}BM$ (4% IMe)	825	4.04	37	1.23
TQ1:$PC_{61}BM$ (3% IEt)	804	9.07	52	3.76
TQ1:$PC_{61}BM$ (4% IEt)	685	9.16	45	2.83
TQ1:$PC_{61}BM$ (3% DIMe)	823	12.43	44	4.53
TQ1:$PC_{61}BM$ (4% DIMe)	769	9.22	47	3.17

Therefore, the information obtained from current density-voltage curve (Figure 5.5 and Table 5.4) indicates that the optimum performance of TQ1:$PC_{61}BM$ solar cells were obtained when the percentage compositions of iodomethane, iodethane and di-iodomethane is 3% (v/v) of the host solvent (o-dichlorobenzene).

5.3.2 J-V Characteristics of the Optimized Organic BHJ Solar Cells

According to the J–V curves of Figure 5.6 and the extracted photovoltaic parameters in Table 5.5, the device without solvent additive (pristine) shows V_{oc} of 795 mV, J_{SC} of 7.32 mA/cm^2, FF of 47%, and power conversion efficiency (PCE) of 2.71%. After addition of 3% solvent additives, (iodomethane, iodoethane and di-iodomethane) by volume, the photovoltaic performance of these devices were enhanced compared to pristine solar cell. Generally, these pronounced increament in power conversion efficiency is mainly due to the increase in the J_{sc} value.

In TQ1:PC_{61}BM BHJ solar cells with optimized 3% (v/v) solvent additives (iodomethane, iodoethane and di-iodomethane), the main cause for the increasing the short-circuit current density, i.e. from 7.32 mA/cm^2 (for pristine) to 8.41, 9.07 and 12.43 mA/cm^2 respectivelly, is most probably related to the improvement of absorbance (Figure 5.2) and formation of optimum interface contact area in the range of exciton dissociation of ~10 nm. The later can be evidenced from the highly quenched photoluminescence of the polymer film (Figure 5.3) up on addition of the solvent additives to pristine blend. Generally, an increment of the current density collected at the electrodes can be attributed to different causes, might be, from an increase in photon absorption, charge dissociation, and charge transport to the electrodes and charge collection [66]. As evidenced by UV-visible characterization, more visible photons absorption that increased from IMe, IEt and DIMe respectively which contributed to the increase in the photocurrent. In the TQ1:PC_{61}BM procesed with iodomethane, and di-iodomethane, organic BHJ device FF decreased slightly from 47% to 46% and 44%, respectively (i.e. 1 and 3% in relative).

This slight reduction in fill factor are generally caused by high series resistance from poor contacts between organics and electrodes. Besides, and more interestingly, the highest overall PCE (4.53%) with J_{sc} of 12.43 mA/cm^2, V_{oc} of 823 mV and a FF of 44% was observed in di-iodomethane processed device. This highly improved PCE in di-iodomethane compared to the corresponding iodomethane might be because of the presence of extra polarisable iodine atom in di-iodomethane that creates strong interaction to solublize $PC_{61}BM$ aggregates and its high boiling point (slow drying effect) than iodomethane that ultimately led to enhanced crystallinity of TQ1 chains. Therefore, this indicates di-iodoalkanes results in higher V_{oc}, J_{sc}, and PCE than iodoalkanes with the same chain length (Table 5.5). In contrast, The PCE (3.76%) was exhibited by devices made using iodoethane is higher than that of iodomethane. The main reason for this is the increase in alkyl chain, which leads to strong interaction to solublize $PC_{61}BM$ aggregates. Therefore, it can be observed that as the alkyl chain length increases from iodomethane to iodoethane, the photovoltaic parameters (J_{sc}, FF and PCE) increases significantly.

The open-circuit voltage of organic solar cells is determined by the energy difference between the highest occupied molecular orbital (HOMO) of the electron donor and the lowest unoccupied molecular orbital (LUMO) of electron acceptor material. Therefore, any change in the HOMO level of the donor and/or LUMO level of the acceptor results into a change of V_{oc}. As shown in Figure 5.6 and Table 5.5, for the TQ1:$PC_{61}BM$ device, the V_{oc} of the devices are enhanced from 795 mV (pristine) to 808, 804 and 823 mV after addition of IMe, IEt, and DIMe, respectively. Therefore, this ample enhancement might be due to the optimized energy level alignment of the TQ1 with $PC_{61}BM$, low charge-carrier recombination rates or a small degree of energetic disorder (homogeneous

broadening of HOMO or LUMO energy levels) [67]. Devices processed in di-iodomethane exhibited a relatively higher V_{oc}, which is mainly attributed to optimum phase separation resulting in large decrease in recombination. The presence of this additive may also increases the crystalline domain size of TQ1 and hence the planar conjugation and such systems are characterized by higher HOMO-LUMO gap [68]. This result is in consistent with the complete response in J_{sc} of the device since the development of ordered domains results good donor-acceptor interface and hence the photo induced charge transfer is increased. On the other hand, devices processed in iodoethane exhibited an insignificant reduction of V_{oc} compared to iodomethane. This might be as a result of its ordered crystalline aggregation development that facilitates the π-system of TQ1 intermolecular interaction and delocalization which leads to insignificant lowering of the energy gap between HOMO level of TQ1 and LUMO level of $PC_{61}BM$. It is known for a long time that reduction in V_{oc} caused by trapping minority carriers, leading to an increase in recombination [69]. Furthermore, mechanisms which reduce V_{oc} of device could be the formation of a band structure instead of molecular energy levels (or alternatively the splitting of the HOMO and LUMO levels) due the strong interchain–interlayer interactions originating from the relatively high ordering of TQ1 in the solvent processed films, which thus leads to a reduced effective “bandgap” relative to the HOMO-LUMO difference.

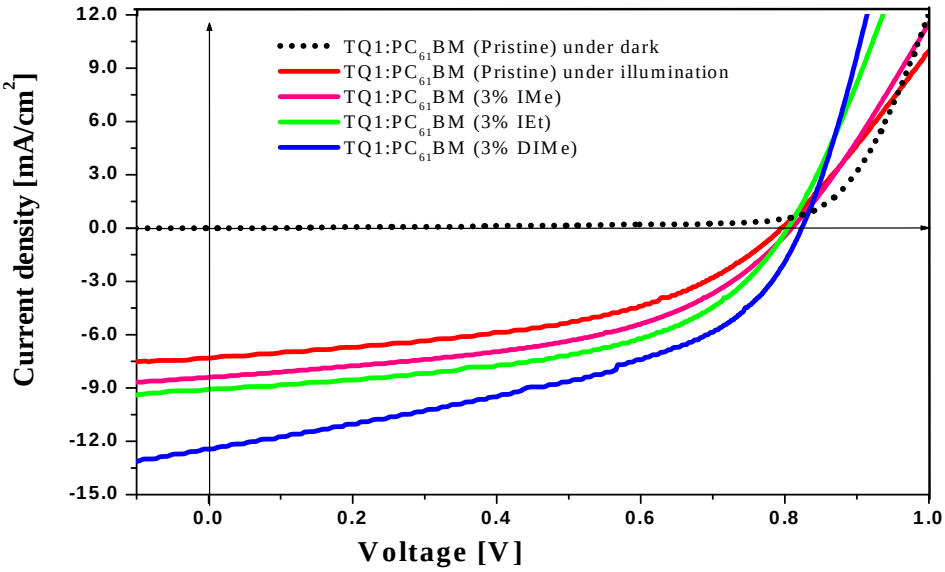

Figure 5.6: The J-V characteristics of glass/ITO/PEDOT-PSS/TQ1:$PC_{61}BM$/Al based BHJ solar cell with different solvent additives: none (red), 3% IMe (pink), 3% IEt (green) and 3% DIMe (blue) in the dark (black dot line) and under white light illumination.

Table 5.5: Photovoltaic parameters of TQ1:$PC_{61}BM$ BHJ solar cells spin-coated from pure o-dichlorobenzene and o-dichlorobenzene containing 3% (v/v) of iodomethane (IMe), iodoethane (IEt) and di-iodomethane (DIMe) solvent additives under 100 mW/cm^2 illumination.

Conditions	V_{oc} (mV)	J_{sc} (mA/cm^2)	FF (%)	PCE (%)
TQ1:$PC_{61}BM$ (pristine)	795	7.32	47	2.71
TQ1:$PC_{61}BM$ (3% IMe)	808	8.41	46	3.28
TQ1:$PC_{61}BM$ (3% IEt)	804	9.07	52	3.76
TQ1:$PC_{61}BM$ (3% DIMe)	823	12.43	44	4.53

5.4 Spectral Response of the Optimized Organic BHJ Solar Cells

The dependence of the photovoltaic performance on the solvent additives was further confirmed by the incident monochromatic photon to current conversion efficiency (IPCE) measurement of the devices (Figure 5.6). In general, the IPCE curves of the devices with IMe, IEt and DIMe has showed better photon-to-current conversion compared to the pristine solar cells. This is also in agreement with the enhancement of the absorption intensity of the blends with the solvent additives. As shown in Table 5.6, with adding IMe, IEt and DIMe, the IPCE maximum increases from 19.54% (Pristine) to 33.45 %, 54.00% and 54.24% at wavelength of 610 nm, respectively. Therefore, this significant increase of IPCE indicates that more photons are absorbed by the active materials processed in the solvent additives and ultimatlly converting into useful form of current. The enhancement of IPCE (%) is in consistent with increase in J_{sc} of solar cells made from blends containing the solvent additives.

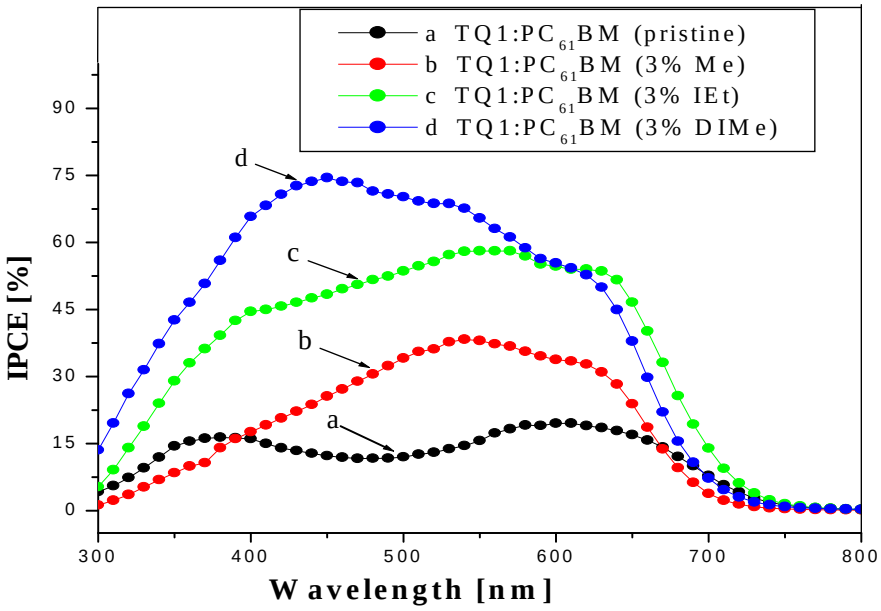

Figure 5.7: Incident photon-to-current conversion efficiency (IPCE) of the glass/ITO/PEDOT-PSS/TQ1:PC_{61}BM/Al, (~99 nm) devices processed in pure o-DCB, and o-DCB containing 3% (v/v) of solvent additives: a) Pristine (0%), b) IMe c) IEt, and d) DIMe.

Table 5.6: Maximum IPCE (%) of glass/ITO/PEDOT-PSS/TQ1:PC_{61}BM/Al, (~99 nm) BHJ solar cell devices at the maximum absorption wavelength.

Condition	IPCE (%) at 610 nm
TQ1:PC_{61}BM (Pristine)	19.54
TQ1:PC_{61}BM (3% IMe)	33.45
TQ1:PC_{61}BM (3% IEt)	54.00
TQ1:PC_{61}BM (3% DIMe)	54.24

6. CONCLUSIONS

In this study, we have shown the effects of low boiling point solvent additives (iodomethane, iodoethane and di-iodomethane) on performance of TQ1:$PC_{61}BM$ based solar cells. The optimized composition of the solvent additives used was 3% (v/v) of the host solvent (o-dicholorobenzene). Interestingly, bulk heterojunction devices processed from iodomethane, iodoethane and di-iodomethane solvent additives in general exhibited enhanced PCE (3.28%, 3.76%, and 4.53%, respectively) as compared to devices without solvent additive (2.71%). Despite the good performance obtained from iodoethane, increasing the chain length of alkyliodide additives have increased the efficiency of TQ1:$PC_{61}BM$ bulk heterojunction solar cells. Moreover, devices made from a blend containing di-iodomethane additive exhibited enhanced J_{sc}, V_{oc}, and PCE as compared to device with iodomethane solvent additive. From this, it can be conclude that di-iodoalkanes results in higher V_{oc}, J_{sc}, and PCE compared to iodoalkanes with the same chain length. Generally, processing BHJ layers with these solvent additives has proven to be an effective strategy toward achieving a nearly ideal BHJ morphology correlated with high efficiency.

The absorption spectra of TQ1:$PC_{61}BM$ blended film processed in o-dichlorobenzene containing di-iodomethane showed a relative red-shift at the characteristic TQ1 absorption band as compared to the pristine (TQ1:$PC_{61}BM$) blend. In contrast, the bulk heterojunction devices fabricated from iodomethane and iodoethane has not significantly affected the absoption band postion as compared to the absoption band of pristine (Figure 5.2 and Table 5.2). However, from the enhanced intensity of the peaks, it is proven that

the crystallinity was indeed improved after the use of the solvent additives from iodomethane and iodoethane.

Moreover, the photoluminesence spectra intensity of TQ1:$PC_{61}BM$ films processed in o-dichlorobenzene containing 3% (v/v) IMe, IEt and DIMe decreases as compared with TQ1:$PC_{61}BM$ films processed in o-dichlorobenzene (pristine), respectively. This strong reduction of the PL intensity indicates that the solvent additives have created optimum interface area between donor and acceptor that largely enhances charge transfer before decaying radiatively or non radiatively.

It is known that the conventional rule for utilization of solvent additives in BHJ organic photovoltaic cells is possesing a higher boiling point (lower vapor pressure) than the parent solvent. This lets the additives can stay longer in the film giving rearengement time for the blend that control morphology. However, in this study we have shown that the low boiling point solvent additives have largely enhanced the performance of organic solar cells based on TQ1:$PC_{61}BM$ BHJ solar cells.

REFERENCES

1. Key World Energy Statistics, *I. Ene. Agency*, Paris, 2006, 46.

2. R.D. Costa, F. Lodermeyer, R. Casillas, D.M. Guldi, *Ene. Environ. Sci*., 2014, **7**, 1281.

3. H.J. Snaith, *J. Phys. Chem. Lett.*, 2013, **4**, 3623.

4. G. Li, R. Zhu, Y. Yang, *Nat. Photonics*, 2012, **4**, 153.

5. J. Heo, S. Im, J. Noh, T.N. Mandal, C. Lim, J.A. Chang, Y.H. Lee, H. Kim, A. Sarkar, M.K. Nazeeruddin, M. Gratzel, S. Seok, *Nat. Photonics*, 2013, **1**, 80.

6. L. Etgar, *Materials*, 2013, **6**, 445.

7. B. Cai, Y. Xing, Z. Yang, W. Zhang, J. Qiu, *Ene. Environ. Sci*., 2013, **6**, 1480.

8. I. Chung, B. Lee, J. He, R.H. Chang, M.G. Kanatzidis, *Nature*, 2012, **486**, 485.

9. T. Saga, *Asia materials*, 2012, **2**, 96.

10. M.P. Lumb, M.K. Yakes, J. Abell, J. G. Tischler, C.G. Bailey, I. Vurgaftman, J. R. Meyer, L.C. Hirst, K.J. Schmieder, S.I. Molina, F.P. Delgado, J.G.J. Adams, G. Hillier, N.J.E. Daukes, R.J. Walters, *Proc. of SPIE*, 2014, **1**, 8981.

11. Z. Bao, A. Dodabalapur, A.J. Lovinger, *Appl. Phys. Lett*., 1996, **69**, 4108.

12. M.C. Scharber, N.S. Sariciftci, *Progress in Polymer Sci*., 2013, **38**, 1929.

13. Y. Liang, Z. Xu, J. Xia, S.T. Tsai, Y. Wu, G. Li, C. Ray, L. Yu, *Adv. Mater*., 2010, **22**, 135.

14. S.W. Hur , T.W. Kim, D.H. Chung, H.S. Oh, C.H. Kim, J.U. Lee, J.W. Park, *Appl. Phys*., 2004, **45**, 627.

15. Y. Liu, C.C. Chen, Z. Hong, J. Gao, Y.M. Yang, H.Z.L. Dou, G. Li, Y. Yang, *Solar Ene. and Photo. Tech. Sci. Repot*., 2013.

16. M.F. Rahman, Jannat, M.S. Hossain khan, *I.J. Scientific & Engin. Res.*, 2013, **4**, 2229

17. A. Chaubey, B.D. Malhotra, *Biosensors and Bioelectronics*., 2002, **17**, 441.

18. R. Janmanee, S. Chuekachang, S. Sriwichai, A. Baba, S. Phanichphant, *J. Nanotech*. 2012, 950.

19. M. Ates, T. Karazehir, A.S. Sarac, *Current Physical Chemistry*, 2012, **2**, 224.

20. K.M. Molapo, P.M. Ndangili, R.F. Ajayi, G. Mbambisa, S.M. Mailu, N. Njomo,M. Masikini, P. Baker, E.I. Iwuoha, *J. Electrochem. Sci*., 2012, **7**, 11859.

21. A.O. Patil, A.J. Heeger, F. Wudl, *Chem. Rev*, 1988, **88**, 183.

22. A.G.M. Diarmid, *Angew. Chem. Int. Ed*., 2001, **40**, 2581.

23. P. Bruyn, D.J.D. Moet, P.W.M. Blom, *Organic Electronics*, 2010, **11**,1419.

24. A.K. Bakhshi, G. Bhalla, *J. Sci. Ind*., 2004, **63**, 715.

25. H. Hoppe, N.S. Sariciftci, *J. Mater. Res*., 2004, **19**, 1924.

26. C. Deibel, V. Dyakonov, *Rep. Prog. Phys.*, 2010, **73**, 096401.

27. K.S. Nalwa, J.A. Carr, R.C. Mahadevapuram, H.K. Kodali, S. Bose, Y. Chen, J.W. Petrich, B. Ganapathysubramanian, S. Chaudhary, *Ene. Environ*., 2012, **5**, 7042.

28. H. Spanggaard, F.C. Krebs, *Solar Ene. Mater. & Solar Cells*, 2004, **83**, 125.

29. A.J. Moulé, J.B. Bonekamp, K.Meerholz, *J. Appl. Phys.*, 2006, **100**, 094503.

30. T. Xu, L. Yu, *Materials*, 2014, **17**, 11.

31. G. Yu, J. Gao, J. C. Hummelen, F. Wudl, A. J. Heeger, *Science*, 1995, **270**, 1789.

32. A.J. Heeger, *Rev. Mod. Phys*., 2001, **73**, 681.

33. C. Bounioux, E.A. Katz, R.Y. Rozen, *Polym. Adv. Technol*. 2012, **23**, 1129.

34. T.Q. Nguyen, I.B. Martini, J. Liu, B. J. Schwartz, *J. Phy. Chem. B*, 2000, **104**, 237.

35. Y. Wang, A. Suna, *J. Phy. Chem. B*. 1997, **101**, 5627.

36. L.M. Chen, Z. Xu, Z. Hong, Y. Yang, *J. Mater. Chem*., 2010, **20**, 2575.

37. C. Zhang, J. Zhang, Y. Hao, Z. Lin, C. Zhu, *J. App. Phy.*, 2011, **110**, 064504.

38. D.M. Tobnaghi, M. Sojoudi, R. Madato, *Tech. J. Engin. and App. Sc*i., 2013, **3**, 3854.

39. U.T. Kute, P.S. Ratnaparkhi, *I.J. Adv. Research in Engin. and Appl. Sci*.., 2013, **2**, 2278.

40. K.M. Kandil, M.S. Altouq, A.M. Al-asaad, L.M. Alshamari, I.M. Kadad, A.A. Ghoneim, *Smart Grid and Rev. Energy*, 2011, **2**, 375.

41. N. Ulapane, S. Abeyratne, P. Binduhewa, C. Dhanapala, S. Wickramasinghe, N. Rathnayake, *I.J. Soft Comput. and Software Engin.*, 2012, **2**, 2251.

42. S.H. Lee, D. Lee, W. S. Hwang, E. Hwang, D. Jena, W. Jong Y, *Appl. Phys. Lett.*, 2014, **104**, 193113.

43. G.P. Smestad, F.C. Krebs, C.M. Lampert, C.G. Granqvist, K.L. Chopra, X. Mathew, H. Takakura, *Solar Ene. Mater. and Solar Cells*, 2008, **92**, 371.

44. H. Derouiche, S. Saidi, A.B. Mohamed, *Smart Grid and Renew. Ene.*, 2011, **2**, 278.

45. M. Scarongella, A.A. Paraecattil, E.B.Domingo, J.D. Douglas, T.M. Ward, M. Heeney, J.E. Moser, M. Leclerc, J.M.J. Fr´echet, N. Stingelin, N. Banerji, *J. Mater. Chem. A*, 2014, **2**, 6218.

46. R. Kroon, M. Lenes, J.C. Hummelen, P.W.M. Blom, B.D. Boer, *Polymer Rev.*, 2008, **48**, 531.

47. J.C. Bernède, *J. Chil. Chem. Soci.*, 2008, **53**, 1549.

48. J. Peet, N.S. Cho, S.K. Lee, G.C. Bazan, *Macromolecules*, 2008, **41**, 8655.

49. W.A. Hammed, R. Yahya, A.L. Bola, H.N.M.E. Mahmud, *Energies*, 2013, **6**, 5847.

50. B.C. Thompson, J.M.J. Frechet, *Angew. Chem. Int. Ed.*, 2008, **47**, 58.

51. G. Li,Y. Yao, H. Yang, V. Shrotriya, G. Yang, Y. Yang, *Adv. Funct. Mater*., 2007, **17**, 1636.

52. J.D.A. Lin, J. Liu, C. Kim, A.B. Tamayo, C.M. Proctor, T.Q. Nguyen, *R. Soci. Chem. Adv.*, 2014, **4**, 14101.

53. T. Salim, L.H. Wong, B. Br€auer, R. Kukreja, Y.L. Foo, Z. Bao, Y.M. Lam, *J. Mater. Chem.*, 2011, **21**, 242.

54. S.J. Lou, J.M. Szarko, T. Xu, L. Yu, T.J. Marks, L.X. Chen, *J. Ame. Chem. Soci.*, 2011, **133**, 20661.

55. J.S. Kim, J.H. Park, J.H. Lee, J.Jo, D.Y. Kim, K. Cho, *App. Phys. Lett.*, 2007, **91**, 0003.

56 C. Gong, H.B. Yang, Q.L. Song, Z.S. Lu, C.M. Li, Solar Ene. Mater. & Solar Cells, 2012, **12**, 0927.

57. W. Jang, Y.Q. Yang, J.S. Kim, S.H. Lee, Y.S.Lee, Bull. Korean Chem. Soci., 2013, **34**, 1887.

58. J.E. Carle, B. Andreasen, T. Tromholt, M.V. Madsen, K. Norrman, M. Jørgensen, F.C. Krebs, *J. Mater. Chem.*, 2012, **22**, 24417.

59. M. Nam, J. Huh, W. H. Jo, *Solar Ene. Mater. & Solar Cells*, 2010, **94**, 1118.

60. K. Hong, S.H. Kim, C. Yang, T.K. An, H. Cha, C. Park, C.E. Park, *Organic Electronics*, 2011, **12**, 516.

61. J. Bergqvist, C. Lindqvist, O. Backe, Z. Ma, Z. Tang, W. Tress, S.Gustafsson, E. Wang, E. Olsson, M. R. Andersson, O. Ingans, C. Muller, *J. Mater. Chem. A*, 20014, **2**, 6146.

62. J. Roncali. *Macromol, Rapid Commun.*, 2007, **28**, 1761.

63. D.H. K. Murthy, A. Melianas, Z. Tang, G. Juska, K. Arlauskas, F. Zhang, L.D.A. Siebbeles, O. Inganäs, T.J. Savenije, *Adv. Funct.Mater.*, 20213, **34**, 4262.

64. I. Botiz, N. Stingelin, *Materials*, 2014, **7**, 2273.

65. H. Kim, S. Ok, H. Chae, Y. Choe, *Nano. Res. Lett.*, 2012, **7**, 56.

66. J.C. Hummelen, J. Knol, L. Sánchez, *Proc. SPIE*, 2001, **4108**, 76.

67. J.C. Blakesley, D. Neher, *Phy. Rev. B*, 2011, **84**, 075210.

68. G.D. Sharma, J.A. Mikroyannidis, R. Kurchania, K.R.J. Thomas, *J. Mater. Chem.*, 2012, **22**, 13986.

69. H.Y. Chen, J. Hou, S. Zhang, Y. Liang, G. Yang, Y. Yang, L. Yu, Y.Wu ,G.L.James C. Blakesley, D. Neher, *Natural Photo.*, 2009, **3**, 649.